Paleoceanography and Paleoclimatology

RESEARCH ARTICLE
10.1029/2018PA003485

Special Section:
The Arctic: An AGU Joint Special Collection

Holocene Changes in Deep Water Circulation Inferred From Authigenic Nd and Hf Isotopes in Sediment Records From the Chukchi-Alaskan and Canadian Beaufort Margins

Charles-Edouard Deschamps[1,2,3], Jean-Carlos Montero-Serrano[1,3], Guillaume St-Onge[1,2,3], and André Poirier[3]

[1]Institut des sciences de la mer de Rimouski, Université du Québec à Rimouski, Rimouski, Québec, Canada, [2]Canada Research Chair in Marine Geology, Institut des sciences de la mer de Rimouski, Université du Québec à Rimouski, Rimouski, Québec, Canada, [3]GEOTOP Research Center, Montréal, Québec, Canada

Abstract The rare earth element concentrations and radiogenic isotope (Sr-Nd-Hf) compositions measured in bulk sediment leachates, together with bulk and clay mineralogical data, from two piston cores recovered in the Canadian Beaufort (AMD0214-02PC) and Chukchi-Alaskan (HLY0501-01JPC) margins were studied to investigate changes in the weathering regimes and deep water circulation during the Holocene. The coupled evolutions of the Nd and Hf isotopic compositions (expressed in epsilon units: εNd and εHf, respectively) are in good agreement with modern seawater and bulk sediment leachate data from Pacific water, Atlantic water, and the Mackenzie River. This agreement supports the idea that boundary exchange and brine formation likely play a significant role in the εNd and εHf values of the bottom waters in the western Arctic Ocean. The εNd and εHf records from the Canadian Beaufort and Chukchi-Alaskan margins reveal changes toward more radiogenic values from the early to late Holocene. Based on the εNd and εHf records, we suggest that the unradiogenic values are not controlled by water mass provenance and mixing but rather by provenance and a change in the weathering regime in the Mackenzie and Yukon drainage basins during the early to mid-Holocene. In contrast, the more radiogenic εNd and εHf values in the Chukchi-Alaskan margin and the mineralogical records in the late Holocene have primarily been controlled by an increase in the contributions of seawater and detrital particles from the Bering Sea via the Bering Strait inflow, which is likely related to major changes in the Pacific Ocean-atmospheric dynamics.

Key Points:
- The first authigenic Nd and Hf isotope records in Holocene sediment cores from the Canadian Beaufort and Chukchi-Alaskan margins are presented
- Unradiogenic Nd-Hf isotopic values between 11 and 4 ka/cal BP are due to major weathering in the drainage basin of the Yukon/Mackenzie Rivers
- Radiogenic Nd-Hf isotopic compositions after 4 ka/cal BP reveal an increase in the Atlantic/Pacific water inflows through the Arctic Ocean

Supporting Information:
- Supporting Information S1

Correspondence to:
J.-C. Montero-Serrano,
jeancarlos_monteroserrano@uqar.ca

Citation:
Deschamps, C.-E., Montero-Serrano, J.-C., St-Onge, G., & Poirier, A. (2019). Holocene changes in deep water circulation inferred from authigenic Nd and Hf isotopes in sediment records from the Chukchi-Alaskan and Canadian Beaufort margins. *Paleoceanography and Paleoclimatology*, *34*, 1038–1056. https://doi.org/10.1029/2018PA003485

Received 3 OCT 2018
Accepted 2 JUN 2019
Accepted article online 7 JUN 2019
Published online 3 JUL 2019

1. Introduction

The Arctic Ocean plays an important role in regulating Earth's climate because (1) its perennial sea ice cover modulates the atmospheric and oceanic heat budget since it reflects a large part of the incoming solar radiation during the summer (albedo) and acts as an insulating shield during the winter (Serreze et al., 2007) and (2) the export of freshwater into the North Atlantic affects the Atlantic meridional overturning circulation by changing the deep water convection (Dickson et al., 2007). The northward flows of Atlantic and Pacific waters (hereinafter referred to as AW and PW, respectively) are the major sources of heat advection toward the Arctic Ocean and strongly affect sea ice distribution (Kinnard et al., 2011; Polyakov et al., 2017). For example, the increase in warm AW to the Arctic over the past 2,000 years seems to be the main factor in sea ice decline (Kinnard et al., 2011). Likewise, the advection of warm PW into the Arctic Ocean induces a greater supply of heat in the western Arctic Ocean and acts as a trigger for sea ice decline in the Chukchi Sea (Shimada et al., 2006; Stein et al., 2017). In this context, paleoceanographic and paleoclimate proxy records from marine sediment cores can provide evidence for the large-scale natural variability in the Arctic deep water circulation during the late Quaternary, against which recent changes can be compared. A better understanding of the past variation in the deep water circulation may help to decipher the processes controlling Arctic climate and sea ice variability.

The neodymium (Nd) and hafnium (Hf) isotope compositions of rocks largely depend on the lithology and crustal age. The Nd and Hf isotope compositions are denoted in epsilon units (εNd and εHf), which reflect the normalization of the $^{143}Nd/^{144}Nd$ and $^{176}Hf/^{177}Hf$ ratios to the chondritic uniform reservoir (Jacobsen & Wasserburg, 1980; Nowell et al., 1998). Hence, low $^{143}Nd/^{144}Nd$ values (εNd of −40) reflect old

continental crust, while high $^{143}Nd/^{144}Nd$ values (εNd of +20) reflect young mantle-derived rocks (Frank, 2002). The variability in the Hf isotope composition in terrestrial rocks is larger than that in Nd, ranging from the most unradiogenic values of εHf ~ −50 in Archean rocks to values as high as +25 in mid-ocean ridge basalt (Zimmermann, Porcelli, Frank, Andersson, et al., 2009). Water masses from different origins therefore acquire distinct regional εNd and εHf signatures derived primarily from riverine continental input, particle-dissolved exchange processes (a process commonly referred to as boundary exchange), and/or benthic sources (e.g., Abbott et al., 2016; Casse et al., 2019; Frank, 2002; Haley et al., 2017; Jeandel et al., 2007; Rickli et al., 2009; Wilson et al., 2013; Zimmermann, Porcelli, Frank, Andersson, et al., 2009; Zimmermann, Porcelli, Frank, Rickli, et al., 2009). Consequently, Nd and Hf can be used as sensitive tracers for both (1) water mass mixing and provenance (Chen et al., 2012; Rickli et al., 2009; Stichel et al., 2012), because both elements' oceanic residence times are shorter than the oceanic mixing time (approximately 1,500 years; Frank, 2002), and (2) detrital provenance changes and continental weathering intensity (Gutjahr et al., 2014; Rickli et al., 2010). Because dissolved trace elements are incorporated by coprecipitation processes during early burial in the top few centimeters of the sediments (Bayon et al., 2004; Haley et al., 2004), the authigenic Nd and Hf signatures can be extracted from ferromanganese (Fe-Mn) oxyhydroxide coatings on marine sediment samples (Bayon et al., 2004; Casse et al., 2019; Chen et al., 2012; Gutjahr et al., 2007). Based on these findings, the analysis of εNd and εHf signatures of authigenic fractions in marine sediments is a powerful tool for assessing late Quaternary changes in water mass provenance and in pathways of weathering inputs.

Taking this into account, a number of studies have investigated the seawater Nd and Hf isotope compositions of past Arctic Intermediate Water extracted from the authigenic Fe-Mn oxyhydroxide fraction of late Tertiary (mid-Miocene) to Quaternary sedimentary records to decipher changes in the weathering regimes and water mass mixing (e.g., Chen et al., 2012; Haley et al., 2008; Horikawa et al., 2015; Jang et al., 2017; Maccali et al., 2013; Meinhardt et al., 2016). Likewise, modern Nd and Hf isotope compositions of seawater in Arctic Ocean basins (Porcelli et al., 2009; Zimmermann, Porcelli, Frank, Andersson, et al., 2009) and premodern authigenic Nd isotope signatures of surface sediments from the Arctic Ocean seafloor (Haley & Polyak, 2013) have been investigated to better present the Arctic Ocean's circulation patterns. Nonetheless, the Holocene variability in the contributions of different water masses to the deeper parts of the western Arctic Ocean is not yet completely understood. Thus, authigenic Nd and Hf isotopic compositions retrieved from sediment cores may provide new clues concerning the evolution of the Holocene deep circulation and climate in the western Arctic Ocean, which may then help to place modern environmental changes in perspective.

In this context, the Nd and Hf isotope signatures and the rare earth element (REE) concentrations obtained from the authigenic Fe-Mn oxyhydroxide fractions, together with the bulk and clay mineralogical analysis, of two sediment piston cores recovered from the Chukchi-Alaskan (core HLY0501-01JPC) and Canadian Beaufort (core AMD0214-02PC) margins are used here to (1) assess changes in the provenance of deep water masses, (2) interpret variations in the dynamics of deep water circulation in terms of paleoenvironmental changes since the last deglaciation, and (3) provide new insights into the potential relationships between changes in erosional inputs and oceanic circulation variations in the western Arctic Ocean since the last deglaciation.

2. Regional Setting

2.1. Oceanic Circulation

The Arctic surface oceanic circulation is related to two main wind-driven circulation systems, which are the anticyclonic Beaufort Gyre (BG) in the western Arctic and the Transpolar Drift (TPD; Darby & Bischof, 2004). On the Beaufort Shelf, the anticyclonic BG pushes both surface currents and sea ice westward at the shelf break. Conversely, closer to shore around the 50-m isobath, the Beaufort Undercurrent transports both PW and AW eastward along the continental margin and into the Amundsen Gulf (Forest et al., 2011). The AW flows through the Fram Strait and the Barents Sea. The depth of the AW is between 200 and 1,000 m and has a temperature above 0 °C (Rudels et al., 2004). The AW circulation is counterclockwise along the margins of the Arctic Ocean. It begins along the Eurasian margin and then separates at the level of the Lomonosov Ridge. A branch of the AW circulation diverges toward the eastern face of the Lomonosov Ridge, and the other branch continues in the Canadian basin (Figure 1; Poirier et al., 2012). The modern

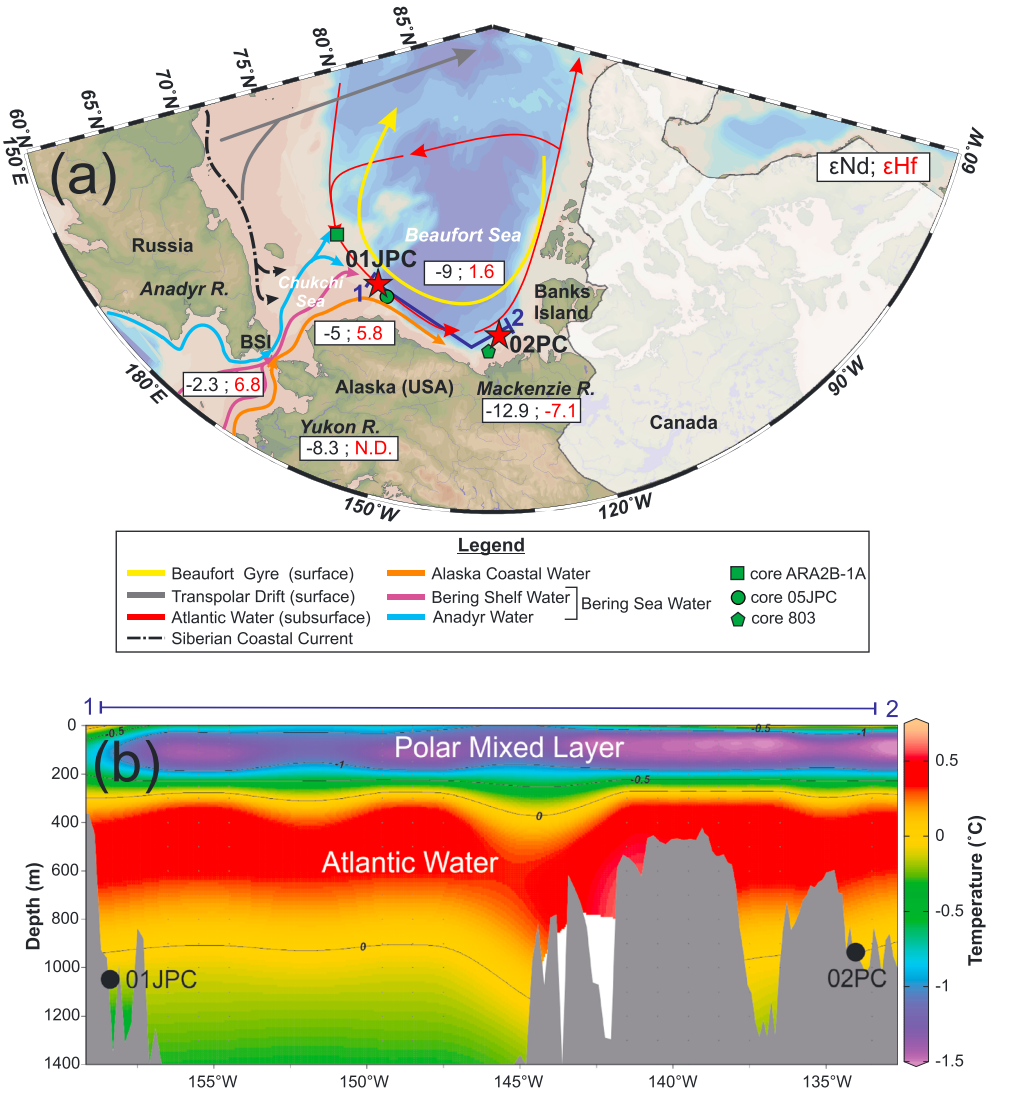

Figure 1. (a) Schematic map of Atlantic water (AW), Pacific water (PW), Transpolar Drift (TPD), and Beaufort Gyre (BG) circulation in the Arctic Ocean and locations of cores 01JPC and 02PC (black circles). The PW drifts eastward in the Beaufort Sea and is known as the Alaskan Coastal Current (ACC). The εNd and εHf values are shown in the map. The Laurentide Ice Sheet at 11.5 ka cal BP is also shown (Dyke, 2004). (b) East-west mean annual temperature profile across the Beaufort-Chukchi slope (transect 1-2 in gray). Core sites are marked by black circles. Temperature data are from Polar Science Center Hydrographic Climatology (PHC, http://psc.apl.washington.edu/Climatology.html).

Nd and Hf isotope signatures of the AW in Arctic Ocean basins have been studied in Porcelli et al. (2009) and Zimmermann, Porcelli, Frank, Andersson, et al. (2009), and the results showed εNd and εHf values of −9 and 1.6, respectively.

The Chukchi Shelf circulation is controlled by an inflow of PW via the Bering Strait (referred to as the Bering Strait inflow or BSI), the Siberian coastal current, and the Atlantic Intermediate Water affecting the northern margin (Figure 1a; Pickart, 2004; Weingartner et al., 2005). PW from the Bering Sea flows into the Chukchi Sea in three major branches (Figure 1a; Pickart, 2004; Pickart et al., 2005; Weingartner et al., 2005; Grebmeier et al., 2006; Okkonen et al., 2009; Danielson et al., 2014; Corlett & Pickart, 2017). The first branch, composed of cold, salty (>32.5) and nutrient-rich Anadyr Water, flows through Hope Valley into Herald Canyon. The third branch, composed of warm, fresh (<31.8) and nutrient-poor Alaskan Coastal Water, flows into Barrow Canyon following the northwestern Alaskan coast in the eastern Chukchi Sea (known as the Alaska Coastal Current or ACC). The second branch, composed of intermediate saline (31.8–32.5) and lower nutrient Bering Shelf Water (BSW), flows between the first and the third branches

through the Central Channel. In general, within the Chukchi Sea, the Anadyr and Bering Shelf waters are both named Bering Sea Water (e.g., Grebmeier et al., 2006; Stein et al., 2017). At interannual time scales, the intensity of the BSI is controlled mainly by the Aleutian Low pressure center's strength and position (Yamamoto et al., 2017). Periods of strengthening of the Aleutian Low pressure center, located over the eastern North Pacific, induce a decrease in the BSI into the Arctic Ocean (Danielson et al., 2014). According to modern hydrographic observations, dense waters (brines) generated at the Chukchi-Alaskan margin during fall/winter sea ice formation can descend to a pycnocline depth of up to 200 m (Pickart et al., 2005; Woodgate et al., 2005). Corlett and Pickart (2017) have shown that PW flows into the Barrow Canyon and forms a slope current called the Chukchi Slope current. The Chukchi Slope current can transport 0.50 Sv of PW westward of Barrow Canyon and can extend into the Atlantic layer (Corlett & Pickart, 2017). The isotopic signature of the PW before entering the Chukchi Sea has been described in Zimmermann, Porcelli, Frank, Rickli, et al. (2009) and Asahara et al. (2012), with εNd values of approximately −2 to −3 and εHf values ranging from 3.5 to 8.6 with a mean value of 6.8. The isotopic signature of the PW throughflow water in the Chukchi Sea is $\varepsilon Nd = -5$ and $\varepsilon Hf = 5.8$ (Haley & Polyak, 2013; Porcelli et al., 2009; Zimmermann, Porcelli, Frank, Andersson, et al., 2009). The change in terms of the isotopic signature of the PW before and after the Bering Strait is possibly due to the influence of runoff from the Yukon and Anadyr rivers and/or so-called boundary exchange with northeastern Bering Sea sediments (Haley & Polyak, 2013; Porcelli et al., 2009). The εNd signature of the Yukon River is $\varepsilon Nd = -8$ to -9 (VanLaningham et al., 2009), and the Hf isotopic signature is still unknown (Horikawa et al., 2010). An increase in the BSI into the Chukchi Sea generally leads to reduced sea ice cover and an increase in sea surface temperature (e.g., McKay et al., 2008; Polyak et al., 2016; Stein et al., 2017). However, as the BSI flows into the Chukchi Sea in three main branches (Figure 1a), the sea ice cover in this region show considerable spatial and temporal variability (Polyak et al., 2016).

2.2. Sedimentation

On the Canadian Beaufort Shelf and the Chukchi Sea, most of the surficial seabed sediments are predominantly composed of Holocene bioturbated gray to olive-gray marine silts and clays (Gamboa et al., 2017; Kobayashi et al., 2016). The modern sedimentation in the Chukchi Sea is believed to be mainly derived from northeastern Siberia, the northeastern Bering Sea (mainly from the Yukon River and to lesser extents from the Aleutian arc and Anadyr River), and the Mackenzie River, whereas the Canadian Beaufort margin sediment originates primarily from the Mackenzie River basin (Asahara et al., 2012; Darby et al., 2011; Deschamps, Montero-serrano, & St-Onge, 2018; Gamboa et al., 2017; Horikawa et al., 2015; Kobayashi et al., 2016; Nelson & Creager, 1977). Smaller Alaskan rivers have a more local impact but may have been a more important sediment source during the early stages of the last transgression (Hill & Driscoll, 2008). During deglaciation and the early Holocene, sediment inputs to the Chukchi-Alaskan and Beaufort margins were presumably higher due to the rising sea level associated with meltwater and iceberg discharge from the retreat of large ice sheets (Deschamps, Montero-serrano, & St-Onge, 2018).

3. Material and Methods

3.1. Sample and Chronology

The sediment core HLY0501-01JPC (hereinafter referred to as core 01JPC; water depth: 1,163 m; location: 72°90′N, 158°42′W) was recovered at the Chukchi-Alaskan margin on board the United States Coast Guard Cutter (USCGC) Healy as part of the 2005 Healy-Oden Trans-Arctic Expedition (Figures 1a and 1b). Core AMD0214-02PC (hereinafter referred as core 02PC; water depth: 998 m; location: 71°22.910′N, 133°34.040′W) was collected on the Canadian Beaufort margin on board the Canadian Coast Guard Ship (CCGS) Amundsen during the 2014 ArcticNet expedition (Figures 1a and 1b). Age models and physical properties of the 01JPC and 02PC sediment cores have been described in Deschamps et al. (2018). The authigenic Fe-Mn oxyhydroxide coatings preserved within these sediment cores likely record past bottom water REE signatures, as reductive diagenesis processes seem to be negligible (Figure S1 in the supporting information; Deschamps, St-Onge, et al., 2018). The sedimentation rate for core 02PC ranged from 2 to 20 cm/ka in the postglacial units, whereas the sedimentation rate in core 01JPC is constant in the postglacial unit (60 cm/ka). Core 01JPC is characterized by a hiatus in the sedimentary sequence at approximately 6 ka cal BP and the deglacial section of the core (Deschamps, St-Onge, et al., 2018). For this reason, only the Holocene units of core 01JPC have been sampled ($n = 11$, resolution of 500 years). Core 02PC spans

the last 13.5 ka cal BP and is characterized by two ice-rafted debris (IRD) intervals between 140 and 160 cm (IRD1) and 320 and 360 cm (IRD2; Deschamps, St-Onge, et al., 2018). In this study, we focus on the last 11.5 ka cal BP ($n = 22$, resolution of 500 years).

3.2. Radiogenic Isotopes and REE Analyses

3.2.1. Bulk Sediment Leaching

Seawater Sr, Nd, and Hf isotopic signatures from authigenic Fe-Mn coatings of the bulk sediment were extracted applying the leaching protocol of Chen et al. (2012). Briefly, 1 g of dried and powdered sediments was rinsed three times with Milli-Q water. Next, Sr, Nd, and Hf contained in the sediment oxyhydroxide fraction were leached for approximately 1 hr in a single step using a dilute reducing and complexing solution consisting of 0.005-M hydroxylamine hydrochloride (HH), 1.5% acetic acid, and 0.03-M Na-EDTA, buffered to pH = 4 with suprapur® NaOH. A buffered acetic acid leach step was omitted since biogenic carbonates are negligible in all sediment samples (Deschamps, Montero-serrano, & St-Onge, 2018). The hydroxylamine hydrochloride and acetic acid mixture was tenfold diluted compared with the method of Gutjahr et al. (2007) to avoid any potential contamination caused by the leaching of clay minerals. During treatment, the sediment samples were gently shaken to enhance the reaction. Leaching method was applied on two sediments sample, one for the REE concentration analyses and the other one for the Nd and Sr chromatographic extraction. The aliquot for REE concentration analysis was evaporated almost to dryness and the residue was redissolved in 1 mL of concentrated HNO_3 and subsequently diluted with Milli-Q water to a total volume of 5 mL.

3.2.2. Sr, Nd, and Hf Separation: Column Chemistry

The Sr, Nd, and Hf were separated from the other elements by applying a single-step ion chromatographic separation (Li et al., 2014). Briefly, the leaching solutions obtained from the previous steps were centrifuged at 5,000 rpm for 8 min. Then, 1 mL of the supernatant solution was passed through a two-layered mixed resin column (70-mm length, 6-mm diameter) with the upper layer containing 1.5 mL of Biorad® AG50W-X12 (200–400 mesh) resin and the bottom layer containing 0.45 mL of Eichrom® LN Spec resin (100–150 μm). Before sample loading for the separation of Sr-Nd-Hf from the sample matrix, the mixed resin column was prewashed with 18 mL of 6 M HCl, 8 mL of 3 M HF, and 4 mL of H_2O in turn. After sample loading and rinsing four times with 0.5 mL of 2.5 M HCl, the column was washed with 13.5 mL of 2.5 M HCl. Most matrix elements (K, Ca, Na, Mg, Al, Fe, Mn, and Ti) and Rb were removed during this step. Then, the Sr fraction was stripped with 5.5 mL of 2.5 M HCl. Part of the HREE (Dy, Ho, Er, Tm, Yb, and Lu) and Ba was then washed out with 3 mL of 2.5 M HCl. Next, the Nd was then isolated from the other REE with 8 mL of 6 M HCl. Finally, the Hf was isolated with 5 mL of 3 M Hf. Then, the Sr, Nd, and Hf fractions were dried on a hotplate at 120 °C to dryness and prepared for isotope measurements.

3.2.3. REE Concentrations and Sr-Nd-Hf Analysis

The REE concentrations (La, Ce, Pr, Nd, Sm, Eu, Gd, Tb, Dy, Ho, Er, Tm, Yb, and Lu) were determined using an inductively coupled plasma-quadruple mass spectrometer (ICP-QMS Agilent 7500c) at ISMER. Procedural blanks (chemistry and mass spectrometry) always accounted for less than 1% of the lowest concentrations measured in the samples. Multielement stock standard solution containing all REE (multielement solution 1, CLMS-1, Spex Certiprep Inc., Quebec, Canada) was used to prepare external calibration and a quality control standard solution containing 4 ng/mL of each REE. ICP-QMS external reproducibility, based on replicate analysis of this control standard solution, was <11% relative standard deviation (1σ) for all REE. The REE abundances were normalized to Post-Archean Australian Shale (PAAS; Taylor & McClennan, 1985) in order to evaluate the REE patterns as given in Maccali et al. (2013) and Du et al. (2016). The fractionation between the light REE (LREE: La-Nd), medium REE (MREE: Sm-Dy), and heavy REE (HREE: Tm-Lu) was investigated using the following indices: HREE/LREE ([Yb + Lu]/[Pr + Nd] and MREE* (2[Tb + Dy]/[Pr + Nd + Yb + Lu]) to investigate the fractionation between LREE, MREE, and HREE (Du et al., 2016; Molina-Kescher et al., 2014).

The Sr isotopic ratios ($^{88}Sr/^{86}Sr$) were measured in dynamic mode on a Thermo Scientific Triton Plus™ multicollector thermal ionization mass spectrometer at GEOTOP (Montreal, Canada). The Sr samples were loaded and analyzed on a single outgassed zone-refined Re filament, layered with a tantalum activator solution (Birck, 1986). Repeated analyses of the NIST-987 standard ($n = 6$) yielded values of 0.710276 ($\pm$0.000021, 2σ reproducibility). This mean value compares well to its certified value of 0.710248

(Weis et al., 2006). The total procedural blanks for Sr were less than 0.5 ng, which is considered negligible compared to the sample yields (>100 ng).

The Nd and Hf isotopic ratios ($^{143}Nd/^{144}Nd$ and $^{176}Hf/^{177}Hf$) were analyzed on a Nu Plasma II instrument, a Multi-Collector Inductively Coupled Plasma Mass Spectrometer (MC-ICP-MS), also at GEOTOP, in dry-plasma conditions using an Aridus II desolvating membrane as the introduction device. The mass-bias correction was made by monitoring $^{146}Nd/^{144}Nd$ (taken to be equal to 0.7219) and $^{176}Hf/^{177}Hf$ (taken to be equal to 0.7325) and by applying an exponential beta-factor correction to the other ratios. Replicate analyses of the standard JNdi-1 and JMC 475 yielded a mean value of $^{143}Nd/^{144}Nd = 0.512108 \pm 0.000020$ (2σ; $n = 20$) and $^{176}Hf/^{177}Hf = 0.282159 \pm 0.000009$ (2σ; $n = 20$), which are within the uncertainty of its certified values of 0.512115 ± 0.000007 (Tanaka et al., 2000) and 0.282160 ± 0.000032 (Nowell et al., 1998), respectively. Hence, no correction has been applied to the Nd and Hf isotope data. The external reproducibility was provided by the repeated measurements of the JNdi-1 (from 0.1 to 0.3 ε units, 2σ; $n = 31$) and JMC 475 (0.5 to 1.3 ε units, 2σ; $n = 31$) standards at the same concentration as the samples. Thus, the analytical error for each sample analysis is taken as the external reproducibility of the JNdi-1 and JMC 475 standard in each analytical session. Some samples have higher uncertainties (up to 0.4 ε units for Nd and up to 9 ε units for Hf; Table S2) because of poorer counting statistics of samples with low Nd and Hf concentrations. The procedural blank values were <0.5 ng for Nd and for Hf and were therefore neglected as they represented less than 0.1% of the Nd and Hf analyzed per sample, respectively. The $^{143}Nd/^{144}Nd$ and $^{176}Hf/^{177}Hf$ isotopic ratios are expressed in ε units (εNd and εHf).

3.3. Bulk and Clay Mineralogical Analyses

Complementary bulk mineral associations were studied by quantitative X-ray diffraction (qXRD) following the method developed by Eberl (2003). Briefly, ~1 g of each sample was spiked with 0.25 g of corundum, and the powder samples were scanned from 5° to 65° two-theta in steps of 0.02° two-theta on a PANalytical X'Pert Powder diffractometer. For the quantification of the major mineralogical components, sediment XRD scans obtained were converted into mineral weight percent (wt. %) using the Excel macro program ROCKJOCK v11 (Eberl, 2003). Then, we used the nonlinear unmixing Excel macroprogram SedUnMixMC (Andrews & Eberl, 2012) to gain a quantitative understanding of the downcore changes in bulk sediment provenance. In addition, clay mineral associations were studied using XRD following established protocols (Bout-Roumazeilles et al., 1999; Montero-Serrano et al., 2009). The separated clay-sized fraction was concentrated by centrifugation and oriented by wet smearing on glass slides. The analyses were run from 2.49° to 32.49° two-theta on a PANalytical X'Pert Powder diffractometer. Three X-ray diagrams were performed, and after the sample was air-dried, ethylene glycol vapor saturation was completed for 12 hr, followed by heating at 490 °C for 2 hr. A semiquantitative estimation of clay mineral abundances (smectite, illite, chlorite, kaolinite, vermiculite, and a chlorite/smectite mixed layer) based on peak areas was performed using the MacDiff® 4.2.5 software (Petschick, 2000). Similar to other Arctic clay mineral studies (Schoster et al., 2000; Wahsner et al., 1999), the clay mineral contents were calculated by using the weighting factors introduced by Biscaye (1965) and calculated to a sum of 100%. Note that bulk and clay mineralogical analyses on sediments for the core 02PC were reported previously (Deschamps, Montero-serrano, & St-Onge, 2018). In this study, based on a previous sediment provenance study in the western Arctic Ocean (Deschamps, Montero-serrano, & St-Onge, 2018), we used the proportion of sediments derived from the Bering Strait and Mackenzie River (SedUnMixMC results), as well as the amorphous silica contents and Log (illite + kaolinite/chlorite + vermiculite) ratio or Log(I + K/C + V) to trace sediment provenance changes over time. The high amorphous silica concentrations in the Chukchi Sea sediments can be interpreted as a major inflow of biosilica-rich PW through the Bering Strait (Jakobsson et al., 2017; Stein et al., 2017). Likewise, the Log(I + K/C + V) ratio allowed us to discriminate between sediments from the Bering Strait (rich in chlorite and vermiculite) and sediments from the Mackenzie River (rich in illite and kaolinite).

4. Results

4.1. Authigenic REE Distribution

The REE concentrations are presented in Table S1. The PAAS-normalized REE of the bulk sediment leachates from both cores reveal an MREE bulge-type pattern (Figure 2), with an enrichment in MREEs compared to HREE and LREE, which is a common pattern in leachates and authigenic material (Abbott et al.,

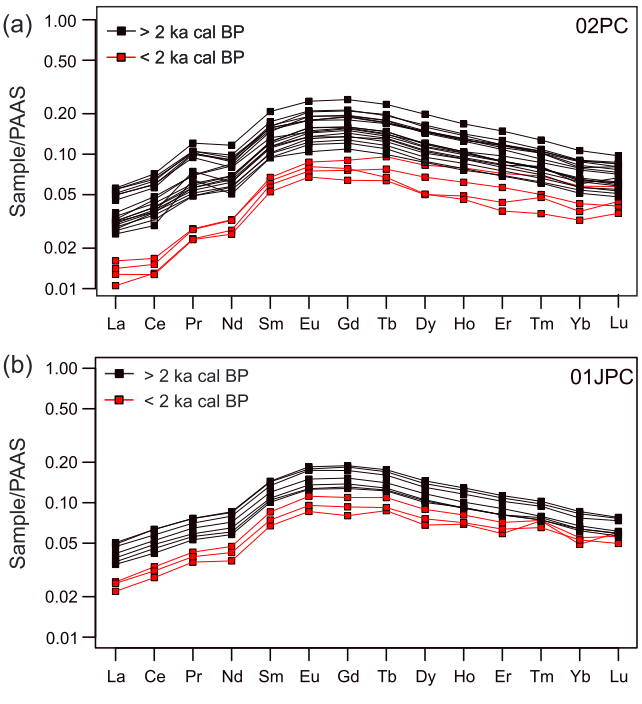

Figure 2. REE patterns normalized to PAAS (Taylor & McClennan, 1985) for the bulk sediment leachate samples from (a) core 01JPC (Chukchi-Alaskan margin) and (b) core 02PC (Canadian Beaufort margin).

2016; Du et al., 2016; Gutjahr et al., 2007). Likewise, to further evaluate the efficiency of our procedure for extracting the authigenic phase, we compared the HREE/LREE ratios to the MREE* values (Figure 3b). The HREE/LREE-MREE* cross plots reveal that all our bulk sediment leachates plot on the Fe-Mn leachate array (Du et al., 2016; Gutjahr et al., 2010). This finding indicates that authigenic Fe-Mn oxyhydroxide coatings control the Nd and Hf signals in our bulk sediment leachates. Furthermore, the significant negative correlation observed between the ΣREE content and εNd values in cores 01JPC ($r = -0.75$) and 02PC ($r = -0.59$) suggests ΣREE enrichment toward more unradiogenic values (Figures 3b).

4.2. Sr, Nd, and Hf Isotope Signatures

The Sr, Nd, and Hf isotope data obtained from the leachates are provided in Table S2. The $^{87}Sr/^{86}Sr$ values obtained from the bulk sediment leachates in cores 01JPC and 02PC range from 0.70922 to 0.70940, with a mean value of 0.70929 ± 0.00004 (Figure 3a). These values are characteristic of the present-day seawater values recorded in the western Arctic Ocean (0.70920; Asahara et al., 2012). In core 01JPC, the εNd values range from −3.7 to −5.7, while the εHf values range from 4.1 to 9.2 (Figures 3d and 4a). In general, the Nd and Hf isotopic signatures in core 02PC are less radiogenic than those in core 01JPC. The εNd values range from −7.6 to −16.8, while the εHf values range from 4.8 to −10.4 (Figures 3d, 4b, and 4c). As shown in Figure 3d, the Nd-Hf isotope values of core 01JPC fall into the seawater array, whereas the data from core 02PC range from the seawater array to the detrital array.

4.3. Bulk and Clay Mineralogical Data

The stratigraphic distributions of the bulk and clay mineralogical data from core 02PC are shown in Deschamps, Montero-serrano, and St-Onge, (2018). The mineralogy of the bulk sediment fraction of core 02PC is dominated by quartz (~22%) and total clays (72%). The clay mineral assemblage of core 01JPC consists of illite (60%), kaolinite (14%), chlorite (14%), vermiculite (8%), and mixed-layer chlorite/smectite (2%). Based on the SedUnMixMC results (Figure 5g), the major source of sediment for core 02PC is related to the Mackenzie River (>80%), and the secondary source is the Canadian Arctic Archipelago (up to 60%). The bulk and clay mineral concentrations of the core 01JPC are presented in Tables S3 and S4, respectively. The mineralogy of the bulk sediment fraction of core 01JPC is dominated by quartz (~20%), total clays (52%), plagioclase (11%), K-feldspar (5%), and amorphous silica (3–14%), and the clay mineral assemblage of core 01JPC consists of illite (27–45%), kaolinite (5–10%), chlorite (10–15%), vermiculite (7–50%), and mixed-layer chlorite/smectite (0–40%). Based on the SedUnMixMC results (Figure 6f and Table S5), the major source of sediment for core 01JPC is related to the northeastern Bering Sea (40–60%), and the secondary source is the Mackenzie River (10–30%).

5. Discussion

5.1. Nd and Hf Isotopic Compositions of Cores 02PC and 01JPC

As shown in Figures 3d, 4b, and 4c, the Nd and Hf isotopic composition of core 02PC displays high variations and ranges between the signatures of the AW (εNd: −9, εHf: 1.6; Zimmermann, Porcelli, Frank, Andersson, et al., 2009) and the modern Mackenzie River (εNd: −12.9, εHf: −7.1; Zimmermann, Porcelli, Frank, Andersson, et al., 2009). From 12 to 6 ka cal BP, the εNd values in core 02PC are clearly similar to those of the Mackenzie River, whereas between 6 and 2 ka cal BP, the Nd isotopic values become more radiogenic and reflect a mixture between those of the AW and the Mackenzie River (Figures 4b and 4c). After 2 ka/cal BP, the εNd values match those of the AW. Similar to the Nd isotopic compositions, the εHf isotopic values in core 02PC transition from a clear Mackenzie River signature (12–6 ka cal BP) to a mixed signature between the Mackenzie River and the AW (6–2 ka cal BP) to predominantly an AW signature after 2 ka cal BP (Figures 4b and 4c).

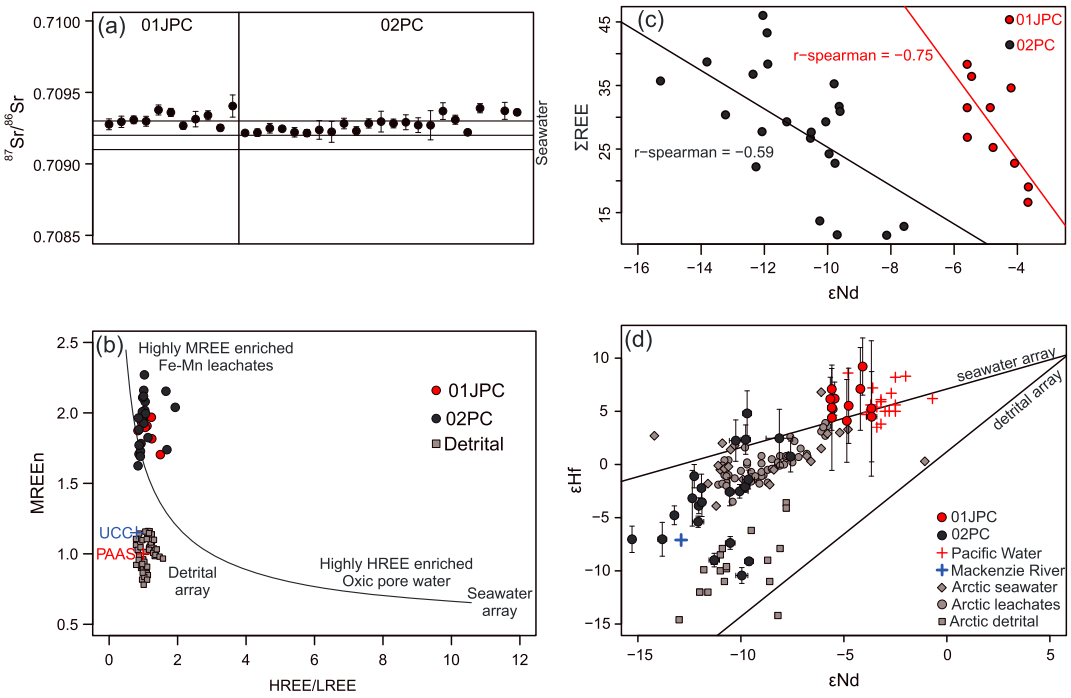

Figure 3. (a) $^{87}Sr/^{86}Sr$ isotope ratios for the bulk sediment leachate samples from cores 01JPC and 02PC; sea water values in the Arctic ocean are shown by the black lines (Asahara et al., 2012). (b) Cross plot of HREE/LREE versus MREE. A mixing line between the most MREE-enriched leachates and the most HREE-enriched oxic pore waters reflect the authigenic-pore water array (Gutjahr et al., 2010). Detrital REE composition of cores 02PC and 05JPC is from Deschamps (2018). (c) Spearman correlation between ΣREE contents and the authigenic εNd values from cores 01JPC and 02PC. (d) Hafnium-neodymium isotope systematics of the bulk sediment leachates obtained in this study together with previously published data and εNd-εHf correlation lines from the literature. Terrestrial and seawater arrays are from Vervoort et al. (1999) and Albarède et al. (1998), respectively. Pacific water, Mackenzie River, and Arctic Sea water values are from Zimmermann, Porcelli, Frank, Andersson, et al., 2009, Zimmermann, Porcelli, Frank, Rickli, et al., 2009), and leachate and detrital values are from Chen et al. (2012).

As shown in Figures 3d and 4a, the Nd isotopic values of core 01JPC between 6 and 4 ka cal BP (εNd ~ −5.5) are very similar to those of the PW recorded in the Chukchi Sea region (Haley & Polyak, 2013; Zimmermann, Porcelli, Frank, Andersson, et al., 2009). This εNd signature likely represents a mixture dominated mainly by unradiogenic Nd isotope compositions from the Yukon River (εNd ~ −8 to −9) and a minor proportion of more radiogenic Nd isotope compositions from the Aleutian arc (εNd ~ +6 to +10; Asahara et al., 2012; Jang et al., 2017). From 1 to 4 ka cal BP, the Nd isotopic values become more radiogenic (εNd ~ −4), shifting toward the eastern Bering Sea Water signatures (εNd = −2 to −3), as estimated from the εNd values of the Fe-Mn oxide fraction (Asahara et al., 2012). Despite the large uncertainties in the Hf isotopic composition, the overall values in core 01JPC match the overall Hf isotopic signature of the PW (Zimmermann, Porcelli, Frank, Andersson, et al., 2009; Zimmermann, Porcelli, Frank, Rickli, et al., 2009; Figure 3d). However, the large external uncertainties associated with the Hf isotopic values in core 01JPC do not allow the determination of Holocene changes in the PW values (Figure S2 and Table S2).

Overall, the εNd and εHf values from the studied sediment leachates represent the bottom seawater values in the Chukchi and Beaufort seas, and the PW (including Bering Sea and Alaskan Coastal waters), AW, and Mackenzie River end-members are clearly distinguishable from one another (Figures 3d and 4). The long-term Nd-Hf isotope variations observed in our bulk sediment leachates, the proportion of sediments derived from the northeastern Bering Sea and Mackenzie River (SedUnMixMC results), the amorphous silica contents, and the Log(I + K/C + V) ratio are discussed below in terms of changes in water sources, shelf-seawater interaction, brine formation, continental input, and possible relationships with both deglacial/Holocene climate variability and relative sea level variations.

5.2. Role of Weathering Regime Changes in the Nd and Hf Isotopic Evolution

Seawater εNd and εHf values are essentially determined by the mixing of different water masses in the open ocean, whereas the interaction between dissolved and detrital fractions is significant near river mouths and

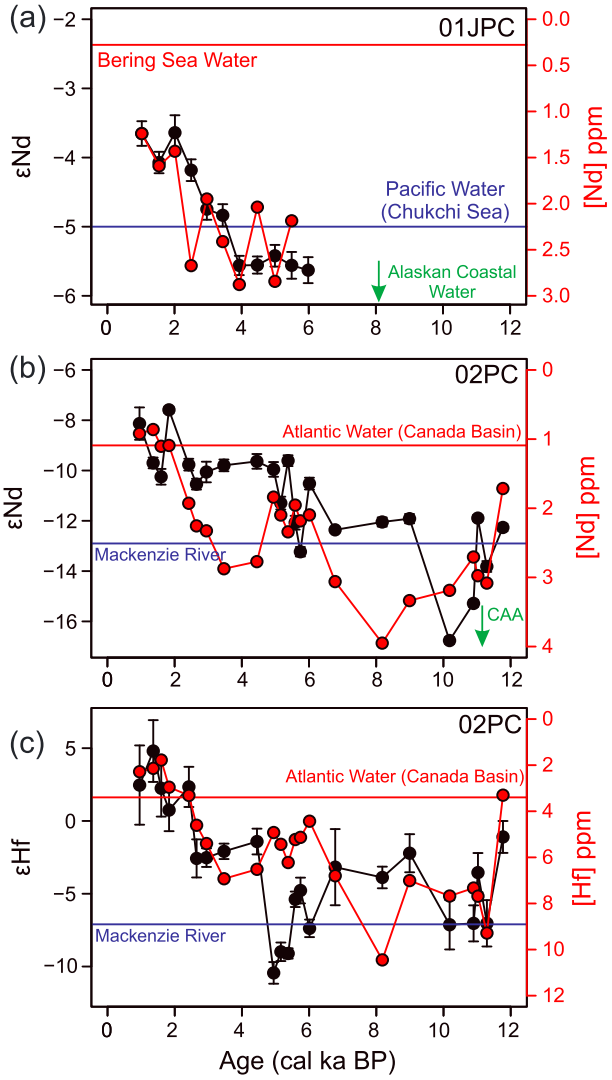

Figure 4. Nd and Hf isotopic evolution of the Arctic deep waters obtained from cores 02PC and 01JPC. Horizontal blue and red lines illustrate modern values of the Bering Sea Water (Asahara et al., 2012; Jang et al., 2017; Zimmermann, Porcelli, Frank, Andersson, et al., 2009), Atlantic water, and Mackenzie River (Porcelli et al., 2009; Zimmermann, Porcelli, Frank, Andersson, et al., 2009). The green arrows indicate the more unradiogenic Nd isotope compositions from the Alaskan Coastal Water (Horikawa et al., 2010, 2015; VanLaningham et al., 2009) and the geological terrains of the Canadian Arctic Archipelago (CAA; Maccali et al., 2018).

continental margins (Chen et al., 2012). Several studies (Lacan & Jeandel, 2005; Pearce et al., 2013; Tachikawa et al., 1999) have discussed the exchange of material between lithogenic particles and seawater along continental margins, a process commonly referred to as boundary exchange, which is thought to play a significant role in controlling the Nd and Hf isotopic and REE compositions of the oceans. In the Arctic Ocean, continental weathering plays an important role in the εNd and εHf values. Indeed, the authigenic Nd and Hf isotopic values of a core recovered on the Lomonosov Ridge that spans the last 14 Myr were more radiogenic than those of the AW, and this difference was greater during glacial periods than during interglacial periods (Chen et al., 2012; Haley et al., 2008). These authors concluded that enhanced continental weathering together with reduced AW inflow during glacial periods was responsible for the more radiogenic values recorded on the Lomonosov Ridge. On the other hand, as described in Porcelli et al. (2009), compared to Atlantic-sourced waters, deep waters in the Canada Basin are enriched in dissolved Nd, apparently through the addition of dissolved Nd from the shelves via brine rejection. Similarly, the seawater Hf concentrations in the Canada Basin are highest at the surface and lowest in the deeper waters, suggesting the addition of river-derived Hf (notably from the Mackenzie River; Zimmermann, Porcelli, Frank, Andersson, et al., 2009).

The detrital εNd values in the northeastern Bering Sea are relatively unradiogenic (~ −7), suggesting that sediments are mainly derived from the Yukon River (εNd ~ −8 to −9) and to a lesser degree from the Aleutian arc (εNd ~ +6 to +10; Asahara et al., 2012; Horikawa et al., 2015; Jang et al., 2017). In contrast, the detrital εNd values in the Mackenzie area are highly unradiogenic (~−15), reflecting material from the North American Craton (Maccali et al., 2018). Thus, the ΣREE concentrations derived from the bulk sediment leachates in cores 02PC and 01JPC increase toward more unradiogenic εNd and εHf values between 12 and 4 ka cal BP, probably reflecting major inputs of both suspended and dissolved loads from the Mackenzie River and Yukon rivers, respectively (Figures 4b and 4c). We hypothesize that the major Nd and Hf inputs associated with enhanced weathering of the Mackenzie (εNd ~ −12.9; εHf ~ −8.1) and Yukon (εNd ~ −8 to −9) river watersheds likely provided a higher contribution of unradiogenic material to cores 02PC and 01JPC during the early to mid-Holocene. Assuming that the addition of Nd and Hf by the rivers could be applied to all REEs, a period of intense weathering in the Mackenzie and Yukon drainage basin may have increased the input of the dissolved ΣREE load and the release of material with unradiogenic Nd and Hf isotopic values into the Beaufort and Chukchi seas (Figures 3c, 3d, and 4). Conversely, the ΣREE concentrations in cores 02PC and 01JPC decreased during the last 4 ka/cal BP, and the Hf and Nd isotopic compositions reflect more radiogenic values. These shifts are probably related to a decrease in the weathering rates in the Mackenzie and Yukon basins and enhanced inflow of PW into the Arctic Ocean (Figures 3c, 3d, and 4).

5.3. Causes of Deglacial-Holocene Seawater εNd and εHf Variations

5.3.1. Canadian Beaufort Margin

In the Canadian Beaufort margin, the Nd and Hf isotopic values from core 02PC (located at a depth of ~1,000 m) exhibit a large range, from −16 to −8 for εNd and from −10 to 5 for εHf, implying major changes in the seawater εNd and εHf since the deglaciation (Figures 5h and 5i). Based on previous radiogenic isotope studies (Chen et al., 2012; Porcelli et al., 2009; Zimmermann, Porcelli, Frank, Andersson, et al., 2009), we suggest that seawater εNd and εHf variation records in core 02PC can be interpreted mainly as the mixing

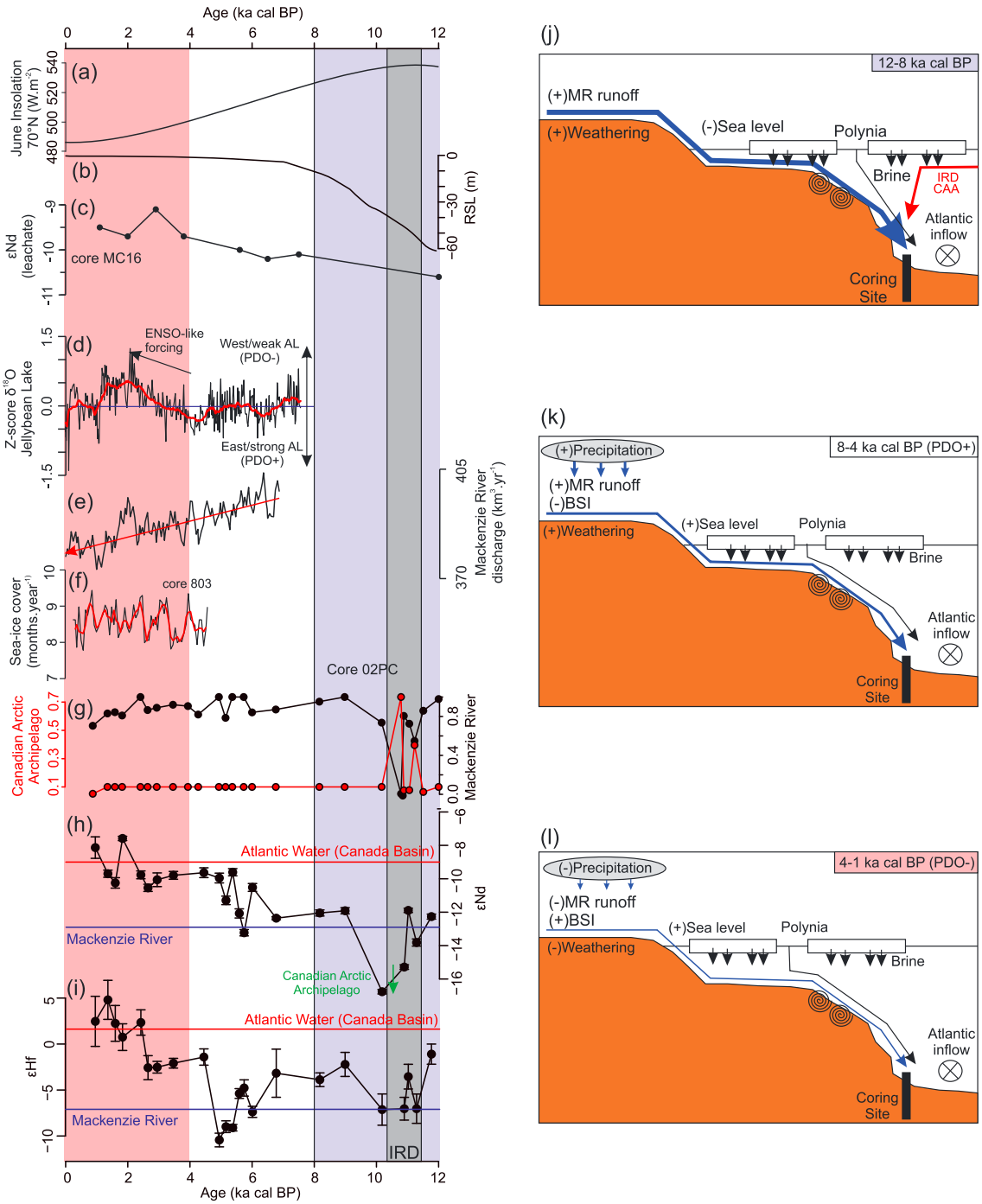

Figure 5. On the left: (a) Mean summer insolation at 70°N (Berger & Loutre, 1991), (b) Global sea level curve (RSL; Lambeck et al., 2014), (c) authigenic εNd records of a sediment core from the Fram Strait (Maccali et al., 2013), (d) Holocene $\delta^{18}O$ records from Jellybean Lake used as a PDO index (Barron & Anderson, 2011), (e) Holocene Mackenzie River discharge based on numerical models (Wagner et al., 2011), (f) Dinocyst-based reconstructions of sea ice cover from the Canadian Beaufort Sea (Bringué & Rochon, 2012), (g) proportion of sediment from the Mackenzie River (black) and the Canadian Arctic Archipelago (CAA; red) in core 02PC (Deschamps, Montero-serrano, & St-Onge, 2018), and (h, i) authigenic εNd and εHf evolution for core 02PC (this study). On the right: schematic illustrations depicting the changes in authigenic εNd and εHf variations in core 02PC between (j) 12 and 8 ka cal BP (light blue), (k) 8 and 4 ka cal BP (white), and (l) after 4 ka cal BP (light red). Spirals indicate sediment resuspension on the Canadian Beaufort slope (Osborne & Forest, 2016).

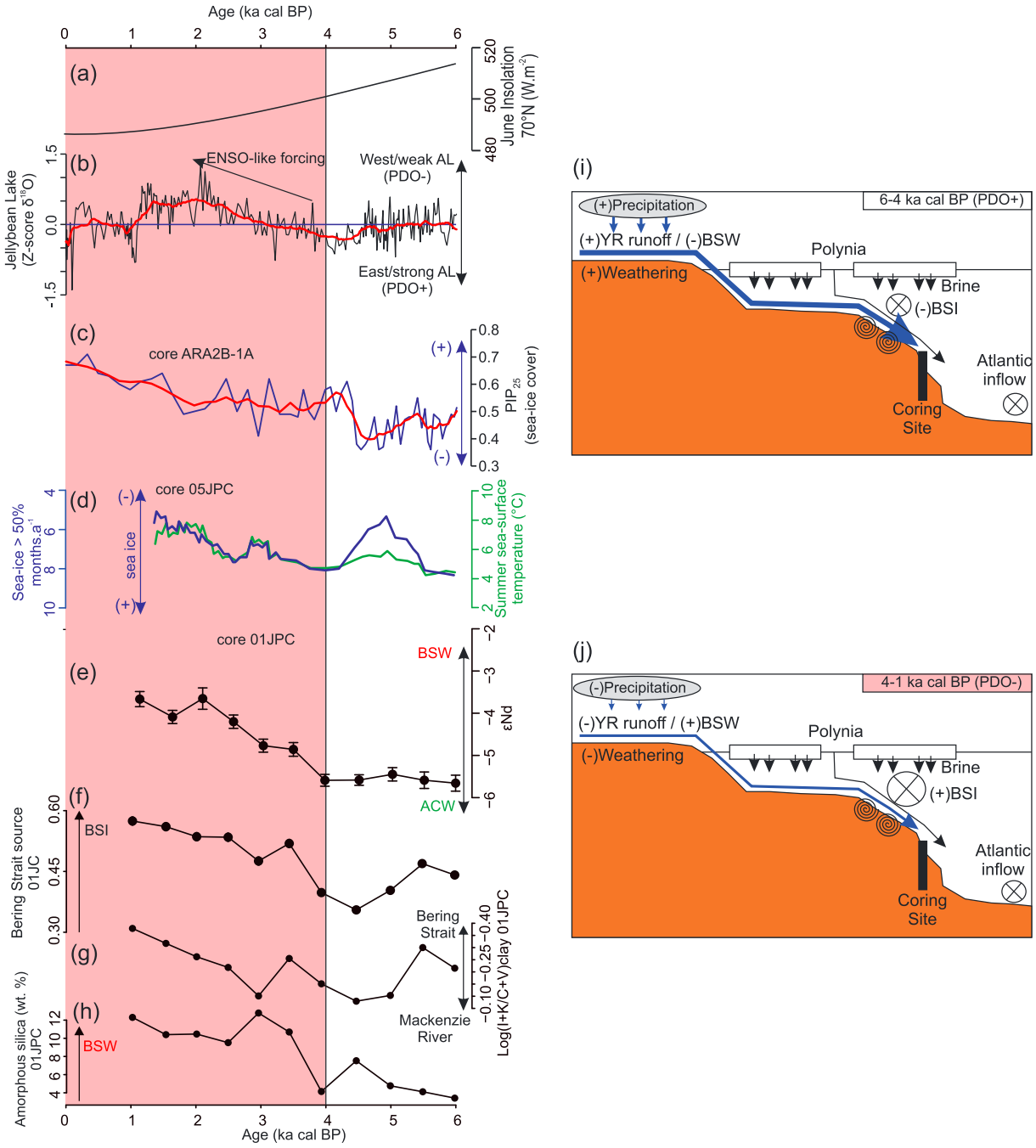

Figure 6. On the left: (a) Mean summer insolation at 70°N (Berger & Loutre, 1991), (b) Holocene $\delta^{18}O$ records from Jellybean Lake used as a PDO index (Barron & Anderson, 2011), (c) sea ice proxy PIP25 (based on brassicasterol) from core ARA2B-1A (Stein et al., 2017), (d) Quantitative reconstruction of past sea surface temperature (red) and sea ice cover (blue) in the core 05JPC based on dinoflagellate cyst assemblages (McKay et al., 2008), (e) authigenic εNd evolution for core 01JPC (this study), (f) proportion of northeastern Bering Sea sediments (this study), (g) Log(I + K/C + V) ratio in core 01JPC, and (h) amorphous silica content in core 01JPC (this study). On the right: (i, j) schematic illustrations depicting the changes in authigenic εNd variations in core 01JPC before 4 ka cal BP (light blue) and after 4 ka cal BP (light red). Spirals indicate possible sediment resuspension on the Chukchi-Alaskan slope (Darby et al., 2009).

of two dominant isotopic end-members, namely, the Mackenzie River and AW (Figures 5h and 5i). The clear Mackenzie River signature recorded in core 02PC during the early Holocene (εNd ~ −13) suggests that enhanced Mackenzie River discharge during this period induced an increase in downslope sediment transfer, resulting in a change in the bottom water Nd-Hf isotope values by particle-dissolved exchange processes (boundary exchange; Haley & Polyak, 2013; Pearce et al., 2013; Tachikawa et al., 1999).

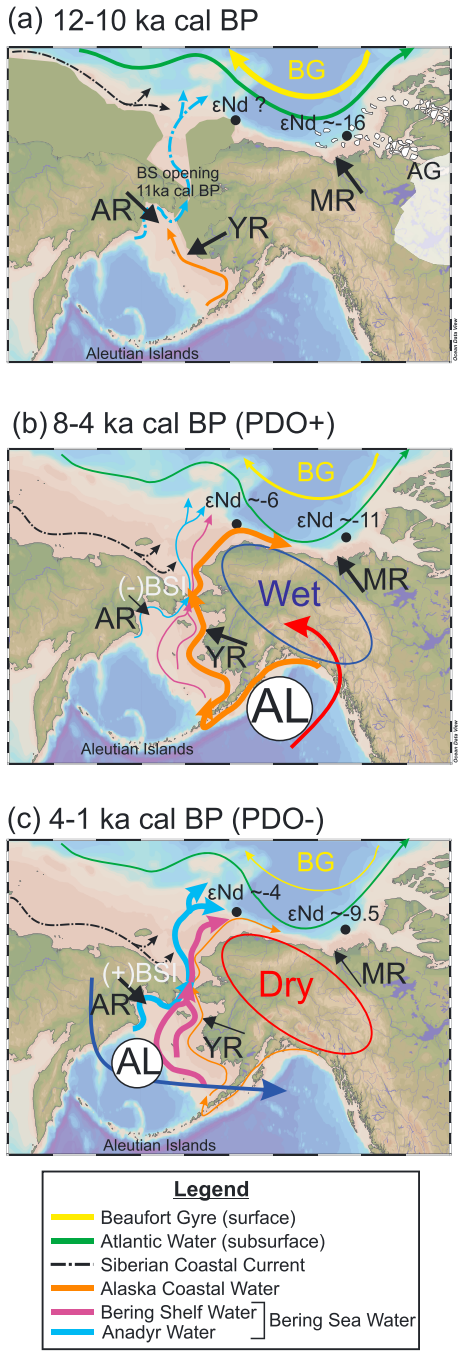

Figure 7. Generalized reconstructions showing the possible changes in the Pacific Water inflow into the western Arctic Ocean during the Holocene (modified from Grebmeier et al., 2006) inferred from the authigenic εNd records of cores 01JPC and 02PC. The Laurentide Ice Sheet position in (a) is about of 11.5 ka cal BP (Dyke, 2004). The Aleutian Low (the bold AL in b and c) patterns according to the PDO-like conditions are also show (Anderson et al., 2016). AR: Anadyr River, YR: Yukon River, MR: Mackenzie River, BG: Beaufort Gyre, AG: Amundsen Gulf.

Alternatively, we cannot rule out that brine rejection resulting from sea ice formation also plays a significant role in the redistribution of dissolved Nd and Hf within the water column (Haley & Polyak, 2013). Therefore, we speculate that the higher release of dissolved and suspended loads with unradiogenic Nd-Hf signatures from the Mackenzie River during the early Holocene, in conjunction with slope convection of brine-enriched shelf waters to the deeper waters, significantly influenced the bottom water Nd and Hf isotope values on the Canadian Beaufort margin. However, as there is no observational evidence for slope convection under 300 m in the Canadian Beaufort Sea (Forest et al., 2015), further investigations are needed to validate this hypothesis. In addition, the most unradiogenic Nd values (εNd ~ −16) at approximately 11 ka cal BP coincide with the dolomite-rich IRD originating from the Canadian Arctic Archipelago (Deschamps, Montero-serrano, & St-Onge 2018; Figures 5g and 5h). The geological terrain in the Canadian Arctic Archipelago is characterize by very unradiogenic Nd isotope values (−14 to −16; Maccali et al., 2018). Thus, the most unradiogenic Nd values recorded in core 02PC during the early Holocene could be explained by (1) the slight dissolution of detrital dolomite during the leaching procedure and/or (2) enhanced dolomite-rich detrital input from the Canadian Arctic Archipelago at this time (Figure 7a) and subsequent particle-dissolved exchange processes (Pearce et al., 2013).

Any major modification in detrital inputs from the Mackenzie River that occurred during the early to middle Holocene could not have been driven by the Laurentide Ice Sheet, which was considerably reduced in size by this time (Dyke, 2004). Wickert (2016) suggested that meltwater inputs to the Mackenzie River ended no later than 11 ka cal BP, when its eastern tributaries were temporarily rerouted eastward due to a combination of ice retreat and glacial isostatic depression. Based on permafrost studies in the Canadian Arctic (Burn, 1997; Dallimore et al., 1996), we hypothesize that the very unradiogenic εNd and εHf values recorded in core 02PC during the early to middle Holocene are more likely the result of a major remobilization of readily erodible rock flour and unconsolidated sediments derived from glacially deformed terrain in the Mackenzie River watershed. The permafrost degradation in the western Canadian Arctic correlates with an enhanced boreal summer insolation during the early Holocene (Figure 5a), which would have increased soil moisture storage and facilitated erosion (Burn, 1997). Furthermore, sedimentary processes in the Beaufort Sea during the early to middle Holocene were strongly influenced by regional sea level variations (Deschamps, Montero-serrano, & St-Onge, 2018). Recently, Cornuault et al. (2018) showed that the εNd record can be influenced by sea level variations. Similarly, the unradiogenic Nd and Hf isotopic values recorded in core 02PC showed a parallel evolution together with the relative sea level variations during the early to middle Holocene (Figure 5b). In this context, we hypothesize that low relative sea level conditions enhanced the relative influence of the Mackenzie River and Canadian Arctic Archipelago (and hence that of isotopic exchange with particles; Pearce et al., 2013) on the Canadian Beaufort Shelf during the early to middle Holocene, leading to more unradiogenic Nd and Hf isotopic values (Figures 5h, 5i, and 7a).

The variability in the weathering regime on the Mackenzie River basin during the middle to late Holocene is likely linked to changes in the precipitation patterns over the western North American continent. Indeed,

previously, investigations on the regional hydrologic responses to atmospheric circulation patterns during the Holocene (e.g., Anderson et al., 2016; Barron & Anderson, 2011) suggest that variations in precipitations on western North America could be controlled by changes in the large-scale atmospheric climate modes, similar to the modern El Niño Southern Oscillation (ENSO) and the Pacific Decadal Oscillation (PDO). An increased sea surface temperature in the North Pacific during a positive PDO (PDO+) phase leads to enhanced water vapor transport over the continent, thus increasing winter precipitation in western North America (Anderson et al., 2016). These conditions are reversed during a negative PDO (PDO−) phases. The transition between the middle to late Holocene (4 ka cal BP) was characterized by a decrease in the boreal summer insolation (Figures 5a), which affected the Northern Hemisphere climate system (Wanner et al., 2008). Several paleoclimate studies based on Alaskan terrestrial records (Anderson et al., 2005, 2016; Barron & Anderson, 2011) and Bering Shelf marine records (Harada et al., 2014; Katsuki et al., 2009) suggest that this transition was characterized by (1) changes from a PDO+ state to a strong PDO− state (Figure 5d) and (2) a decrease in the amount of precipitation linked to a major change in the Aleutian Low intensity and position over the North Pacific. These changes are inferred to have been caused by Pacific Ocean-atmospheric dynamics attributed to an increase in El Niño frequency and a warm eastern tropical Pacific sea surface (Anderson et al., 2016; Liu et al., 2014).

In this context, numerical models of the regional hydrologic responses of the Mackenzie River to large-scale atmospheric circulation patterns suggest a decreasing trend in the freshwater discharges to the Canadian Beaufort margin associated with greatly reduced moisture transport over North America during the middle to late Holocene (Figure 5e), likely driven by a reduction in the boreal summer insolation (Figure 5a) and a predominantly negative PDO-like conditions (Figure 5d; Anderson et al., 2005, 2016; Barron & Anderson, 2011; Wagner et al., 2011; Wanner et al., 2008). Thus, we suggest that this decreased discharge of the Mackenzie River also reduced the inputs of dissolved ΣREE and detrital material with highly unradiogenic Nd and Hf isotopic values to the Canadian Beaufort Shelf (Figure 3c). From 8 to 1 ka cal BP, the isotopic record of core 02PC increases progressively toward more radiogenic values (εNd: −9.5; εHf: 2), similar to the modern values of the AW recorded in the Canada Basin (Figures 5h, 7b, and 7c; Porcelli et al., 2009; Zimmermann, Porcelli, Frank, Andersson, et al., 2009). However, the εNd values observed in the Canada Basin are slightly higher than those of the water entering the North Atlantic (εNd of ~ −10.7; Porcelli et al., 2009). This difference in εNd values probably reflects the influence of the PW (Figure 7c). A εNd value between −9.6 and −9.1 can be obtained by mixing 20% PW and 80% AW (Porcelli et al., 2009). Similar trends have been observed in the Nd isotopic values of a core from the Fram Strait and have been attributed to PW influence (Figure 5c; Maccali et al., 2013). Thus, the changes observed in the authigenic Nd and Hf isotope signatures in core 02PC from 8 to 1 ka cal BP may likely reflect a combination of a decrease in the weathering rates within the Mackenzie River catchment and a relative increase in the influence of the AW and PW masses (Figures 5h, 5i, 7b, and 7c). The enhanced PW inflows are supported by quantitative mineralogical data from the Chukchi Sea, which suggest a gradual increase in sediments delivered from the northeastern Bering Sea by the BSI after 8 ka cal BP (Deschamps, Montero-serrano, & St-Onge, 2018). Furthermore, quantitative reconstructions of past sea surface conditions (temperature, salinity, and the duration of sea ice cover), based on dinoflagellate cyst assemblages and transfer functions (Figure 5f), reveal relatively long-term stable oceanographic conditions during the late Holocene (Bringué & Rochon, 2012). However, the low resolution of our geochemical and mineralogical records prevents any linkage with the short-term variation in past sea surface conditions in the Beaufort Sea. Overall, these results suggest that the modern oceanographic conditions in the Canadian Beaufort Shelf were established during the late Holocene with the concomitant dominance of AW and PW.

5.3.2. Chukchi-Alaskan Margin

In the Chukchi-Alaskan margin, our bulk sediment leachate data from core 01JPC (located at a depth of >1,000 m) show εNd values between 6 and −4 (Figure 6e), similar to the North Pacific throughflow water signatures measured in the Bering Strait (εNd ~ −6 to −4; Porcelli et al., 2009). Note that regional sea level variations did not influence the geochemical record in the Chukchi-Alaskan margin during the middle to late Holocene, as these has been relatively stable during the last 6 ka cal BP (Figure 5b; Lambeck et al., 2014; Deschamps, St-Onge, et al., 2018). However, core 01JPC is located in an area where winter hypersaline polynya waters form through additional salt input from brine rejection along the Alaska coast (Hirano et al., 2018). Based on hydrographic and satellite-derived sea ice production data obtained over the eastern

Chukchi shelf and southeastern Chukchi borderland in conjunction with numerical modeling, Hirano et al. (2018) suggest that winter hypersaline polynya waters over the eastern Chukchi shelf can potentially intrude (via the Barrow Canyon) to depths comparable to or deeper than the AW layer in the Canada Basin. In this context, we hypothesize that particle-dissolved exchange processes with northeastern Bering Sea sediments and/or downflow of brine-enriched Chukchi Sea shelf waters may play a significant role in the distribution of Nd throughout the water column in the Chukchi-Alaskan margin (Haley & Polyak, 2013; Porcelli et al., 2009). These interpretations are in agreement with observations by Haley and Polyak (2013) on the surface εNd distribution in bulk sediment leachates from the Chukchi margin. These authors speculate that modern to premodern distinct radiogenic εNd signals (−6 to −4) observed on the slopes of the Chukchi margin and adjacent borderland could be indicative of PW convection (e.g., via brine rejection) and/or persistent sediment redistribution from the Chukchi shelf. Overall, although we acknowledge that direct observations are needed to validate the deep water convection driven by brines in the Chukchi-Alaskan margin, our results support the hypothesis that both boundary exchange and brine rejection during sea ice formation have probably influenced the distribution of radiogenic isotope (such as Nd and Hf) compositions in western Arctic seawater for the last 6 ka cal BP.

The authigenic εNd record obtained in core 01JPC allows a close look at the changes in the relative contributions between the two main components of the BIS (Figures 6e, 7b, and 7c): (1) Alaskan Coastal Water characterized by more unradiogenic Nd isotope compositions (εNd ~ −8 to −9), which reflect the dissolved Nd inputs from the Yukon drainage basin (e.g., Horikawa et al., 2010, 2015; VanLaningham et al., 2009), and (2) Bering Sea Water, which has more radiogenic Nd isotope compositions (εNd ~ −2 to −3) mainly derived from the western Bering Sea (i.e., coastal water adjacent to the Anadyr region and Bering Shelf; Asahara et al., 2012; Jang et al., 2017). Thus, the more radiogenic εNd values (~ −2) found on the Chukchi shelf can be explained by a high contribution of Bering Sea Water to the BSI and/or less influence of the Yukon River discharge to the Alaskan Coastal waters (Figure 7c). In this context, and as previously discussed, large-scale atmospheric climate modes, such as the PDO, provide a potential mechanistic explanation for correlations between changes in the precipitation patterns over North America and the position of the Aleutian Low in the North Pacific, as well as explaining changes in the BSI (Anderson et al., 2016; Yamamoto et al., 2017). The winter precipitation patterns result from the strength and position of the Aleutian Low, which is strengthened and/or located farther to the east of the North Pacific during a PDO + phase and weakened and/or located more to the west of the North Pacific during a PDO− phase (Barron & Anderson, 2011). In addition, modern data from the Yukon River suggest a positive trend in the annual flow during PDO+ phases, perhaps reflecting the increases in annual precipitation in the interior of Alaska (Brabets & Walvoord, 2009).

Within this context, we hypothesize that the wetter conditions associated with the PDO+ state in conjunction with an enhanced boreal summer insolation during the middle Holocene (Figures 6a and 6b; Anderson et al., 2016; Liu et al., 2014) may have promoted higher weathering rates in the Yukon drainage basin, which is consistent with the high unradiogenic εNd values recorded in core 01JPC (Figures 6e and 7b). Conversely, during the late Holocene, the drier negative PDO-like conditions in western North America (Figure 6b), together with an long-term decrease in boreal summer insolation (Figure 6a), likely reduced the weathering rates in the Yukon drainage basin and therefore produced a relative increase in the contribution of dissolved and detrital loads with more radiogenic values from the Bering Sea Water to the BSI (Figure 7c). Likewise, the decrease in the Log(I + K/C + V) ratio and the relative increase in the proportions of the northeastern Bering Sea sediments (SedUnMixMC results) and amorphous silica (proxy for the BSI intensity; Jakobsson et al., 2017; Stein et al., 2017) in core 01JPC are also in agreement with increases in the BSI during the late Holocene (Figures 6f–6h).

The strength and distribution of BSI water between different branches (Figures 7b and 7c) influences the sea surface temperatures and the spatial and temporal variability of the sea ice cover in the Chukchi Sea (e.g., McKay et al., 2008; Polyak et al., 2016; Shimada et al., 2006; Stein et al., 2017). For example, the results from transfer functions based on dinoflagellate cyst assemblages from the nearby core 05JPC (McKay et al., 2008) suggest a decrease in the duration of sea ice cover and an increase in summer sea surface temperatures after 4 ka cal BP relative to the middle Holocene (between 6 and 4 ka cal BP) in the northeastern Chukchi Sea (Figure 6d). In contrast, based on sea ice biomarker proxy records from two sediment cores from the northwestern Chukchi Sea (ARA2B-1A) and East Siberian Sea (PS72/350-2), Stein et al. (2017)

suggested a significantly increased sea ice extent during the last 4.5 ka cal BP relative to the middle Holocene (Figure 6c). These differences in the sea ice extent in the Chukchi Sea seem to be related to changes in the circulation of the BSI across the Chukchi shelf (Figures 7b and 7c), which is itself modulated by changes in the PDO phase (e.g., Screen & Francis, 2016). Based on numerical models, Winsor and Chapman (2004) suggest that predominantly northeasterly to easterly winds in the northernmost Pacific, usually dominant during PDO+ phases (Zhang & Delworth, 2015), produce an overall reduction in the BSI (induced by an enhanced Aleutian Low) and induce a more northwestward direction to the BSI across the Chukchi shelf edge (Figure 7b). These PDO-like ocean-atmosphere conditions were likely responsible for the sea ice reduction observed in the northwestern Chukchi Sea and East Siberian Sea during the middle Holocene (Stein et al., 2017). Conversely, sustained westerly winds from the northernmost Pacific, usually dominant during PDO− (Zhang & Delworth, 2015), produce an overall intensified BSI (induced by a weakened Aleutian Low) and favor north-northeast diversion of the BSI through the Central Channel and along the Chukchi-Alaskan coast (Figure 7c; Winsor & Chapman, 2004). These atmospheric and oceanographic conditions probably promoted reduced sea ice cover and an increase in sea surface temperatures in the northeastern Chukchi Sea during the last 4 ka cal BP (McKay et al., 2008). Overall, this spatial and temporal variability in the sea ice cover in the Chukchi Sea (Figures 6c and 6d) supports our interpretation of not only an increase in the relative proportion of the Bering Sea Water component of the BSI (Figures 6e–6h) but also major northeastward diversion of the BSI in the Chukchi Sea during the late Holocene (Figure 7c).

Although we recognize that the links with PDO-like ocean-atmosphere interactions warrant further study, evidence of enhanced PDO expression along the northeastern Pacific margins during the late Holocene relative to the middle Holocene (Figure 6b; Barron & Anderson, 2011) is a sufficient explanation of the long-term variability that we observe in our paleoceanographic records. A study with a higher temporal (e.g., centennial to millennial scale) resolution that couples quantitative mineralogy and radiogenic isotope data during this period needs to be performed to provide a better understanding of the relationships among the atmospheric climate mode (e.g., PDO), continental weathering, and the BSI.

6. Conclusion

Using the combined Nd and Hf isotopic record from bulk sediment leachates in two piston cores recovered from the Canadian Beaufort (02PC) and Chukchi-Alaskan (01JPC) margins, we investigated changes in weathering regimes and deep water circulation during the Holocene. Overall, our mineralogical and Nd-Hf isotopic data, together with modeled Holocene Arctic river discharges (Wagner et al., 2011), quantitative reconstructions of past sea surface conditions (McKay et al., 2008; Stein et al., 2017), and hypothesized changes in atmospheric circulation (Barron & Anderson, 2011; Winsor & Chapman, 2004), reveal the following:

1. A clear Mackenzie River and PW isotopic signature at coring sites 02PC and 01JPC at approximately 1,000 m supports the hypothesis that brine rejection during sea ice formation and/or persistent sediment redistribution from the shelf probably plays significant roles in controlling the εNd and εHf values of the bottom waters of the Canadian Beaufort and Chukchi-Alaskan margins.
2. Since the last deglacial period, the Nd and Hf isotopic compositions of bulk sediment leachates from the Beaufort Sea core transition from resembling those of the Mackenzie River end-member to resembling those of the AW end-member. The Mackenzie River-like values are linked to the remobilization of rock flour from glacially deformed terrain in the Mackenzie River watershed and lower sea level conditions during the early Holocene. In the middle to late Holocene, the shift toward AW-like isotopic values is inferred to be the result of a decrease in the Mackenzie River discharge, likely associated with predominantly negative PDO-like conditions.
3. The Nd and Hf isotopic compositions of bulk sediment leachates in the Chukchi-Alaskan margin were controlled by (1) more intense precipitation and weathering in the drainage basin of the Yukon River during the middle Holocene and (2) drier conditions and an increase in the relative contribution of the Bering Sea Water component to the BSI during the late Holocene. This transition seems to have resulted from major changes in atmospheric climate modes induced by a PDO/ENSO-like forcing.

Acknowledgments

We sincerely thank the captains, officers, crew, and scientists on board the USCGC Healy and the CCGS Amundsen for the recovery the cores used in this study. These cores were collected as part of the HOTRAX expedition (USCGC Healy), as well as the CASES and ArcticNet (CCGS Amundsen) programs. We also thank Quentin Beauvais (UQAR-ISMER), Mathieu Babin (UQAR-ISMER), and Adriana Gamboa (UQAR-ISMER and UDO) for their technical support and advice in the laboratory. This research was funded ArcticNet and by the Natural Sciences and Engineering Research Council of Canada (NSERC) through Discovery Grants to J.-C. Montero-Serrano and G. St-Onge, as well as through ship time support for several expeditions (J.-C. Montero-Serrano and G. St-Onge). Finally, thanks to Thomas Barbour and American Journal Experts for reviewing the grammar, the two anonymous reviewers for their constructive review which improve the quality of the manuscript, and Ellen Thomas and Christopher Reinhard for their editorial work. All analytical data presented are available electronically in the supporting information (Tables S1 and S5) and PANGAEA database at https://doi.pangaea.de/10.1594/PANGAEA.897880.

References

Abbott, A. N., Haley, B. A., & McManus, J. (2016). The impact of sedimentary coatings on the diagenetic Nd flux. *Earth and Planetary Science Letters*, *449*, 217–227. https://doi.org/10.1016/j.epsl.2016.06.001

Albarède, F., Simonetti, A., Vervoort, J. D., Blichert-Toft, J., & Abouchami, W. (1998). A Hf-Nd isotopic correlation in ferromanganese nodules. *Geophysical Research Letters*, *25*(20), 3895–3898. https://doi.org/10.1029/1998GL900008

Anderson, L., Abbott, M. B., Finney, B. P., & Burns, S. J. (2005). Regional atmospheric circulation change in the North Pacific during the Holocene inferred from lacustrine carbonate oxygen isotopes, Yukon Territory, Canada. *Quaternary Research*, *64*(1), 21–35. https://doi.org/10.1016/j.yqres.2005.03.005

Anderson, L., Berkelhammer, M., Barron, J. A., Steinman, B. A., Finney, B. P., & Abbott, M. B. (2016). Lake oxygen isotopes as recorders of North American Rocky Mountain hydroclimate: Holocene patterns and variability at multi-decadal to millennial time scales. *Global and Planetary Change*, *137*, 131–148. https://doi.org/10.1016/j.gloplacha.2015.12.021

Andrews, J. T., & Eberl, D. D. (2012). Determination of sediment provenance by unmixing the mineralogy of source-area sediments: The "SedUnMix" program. *Marine Geology*, *291-294*, 24–33. https://doi.org/10.1016/j.margeo.2011.10.007

Asahara, Y., Takeuchi, F., Nagashima, K., Harada, N., Yamamoto, K., Oguri, K., & Tadai, O. (2012). Provenance of terrigenous detritus of the surface sediments in the Bering and Chukchi Seas as derived from Sr and Nd isotopes: Implications for recent climate change in the Arctic regions. *Deep-Sea Research Part II: Topical Studies in Oceanography*, *61-64*, 155–171. https://doi.org/10.1016/j.dsr2.2011.12.004

Barron, J. A., & Anderson, L. (2011). Enhanced Late Holocene ENSO/PDO expression along the margins of the eastern North Pacific. *Quaternary International*, *235*(1-2), 3–12. https://doi.org/10.1016/j.quaint.2010.02.026

Bayon, G., German, C. R., Burton, K. W., Nesbitt, R. W., & Rogers, N. (2004). Sedimentary Fe-Mn oxyhydroxides as paleoceanographic archives and the role of aeolian flux in regulating oceanic dissolved REE. *Earth and Planetary Science Letters*, *224*(3-4), 477–492. https://doi.org/10.1016/j.epsl.2004.05.033

Berger, A., & Loutre, M. F. (1991). Insolation values for the climate of the last 10 million years. *Quaternary Science Reviews*, *10*(4), 297–317. https://doi.org/10.1016/0277-3791(91)90033-Q

Birck, J. L. (1986). Precision K-Rb-Sr isotopic analysis: Application to Rb-Sr chronology. *Chemical Geology*, *56*(1-2), 73–83. https://doi.org/10.1016/0009-2541(86)90111-7

Biscaye, P. E. (1965). Mineralogy and sedimentation of recent deep-sea clay in the Atlantic Ocean and adjacent seas and oceans. *Geological Society of America Bulletin*, *76*(7), 803–832. https://doi.org/10.1130/0016-7606(1965)76[803:MASORD]2.0.CO;2

Bout-Roumazeilles, V., Cortijo, E., Labeyrie, L., & Debrabant, P. (1999). Clay mineral evidence of nepheloid layer contributions to the Heinrich layers in the northwest Atlantic. *Palaeogeography, Palaeoclimatology, Palaeoecology*, *146*(1-4), 211–228. https://doi.org/10.1016/S0031-0182(98)00137-0

Brabets, T. P., & Walvoord, M. A. (2009). Trends in streamflow in the Yukon River basin from 1944 to 2005 and the influence of the Pacific decadal oscillation. *Journal of Hydrology*, *371*(1-4), 108–119. https://doi.org/10.1016/j.jhydrol.2009.03.018

Bringué, M., & Rochon, A. (2012). Late Holocene paleoceanography and climate variability over the Mackenzie slope (Beaufort Sea, Canadian Arctic). *Marine Geology*, *291–294*, 83–96.

Burn, C. R. (1997). Cryostratigraphy, paleogeography, and climate change during the early Holocene warm interval, western Arctic coast, Canada. *Canada Journal of Earth Science*, *34*(7), 912–925. https://doi.org/10.1139/e17-076

Casse, M., Montero-Serrano, J.-C., St-Onge, G., & Poirier, A. (2019). REE distribution and Nd isotope composition of estuarine waters and bulk sediment leachates tracing lithogenic inputs in eastern Canada. *Marine Chemistry*, *211*, 117–130. https://doi.org/10.1016/j.marchem.2019.03.012

Chen, T. Y., Frank, M., Haley, B. a., Gutjahr, M., & Spielhagen, R. F. (2012). Variations of North Atlantic inflow to the central Arctic Ocean over the last 14 million years inferred from hafnium and neodymium isotopes. *Earth and Planetary Science Letters*, *353*, 82–92. https://doi.org/10.1016/j.epsl.2012.08.012

Corlett, W. B., & Pickart, R. S. (2017). The Chukchi slope current. *Progress in Oceanography*, *153*, 50–65. https://doi.org/10.1016/j.pocean.2017.04.005

Cornuault, M., Tachikawa, K., Vidal, L., Guihou, A., Siani, G., Deschamps, P., et al. (2018). Circulation changes in the eastern Mediterranean Sea over the past 23,000 years inferred from authigenic Nd isotopic ratios. *Paleoceanography and Paleoclimatology*, *33*, 264–280. https://doi.org/10.1002/2017PA003227

Dallimore, S. R., Wolfe, S. A., & Solomon, S. M. (1996). Influence of ground ice and permafrost on coastal evolution, Richards Island, Beaufort Sea coast, N.W.T. *Canadian Journal of Earth Sciences*, *33*(5), 664–675. https://doi.org/10.1139/e96-050

Danielson, S. L., Weingartner, T. J., Hedstrom, K. S., Aagaard, K., Woodgate, R., Curchitser, E., & Stabeno, P. J. (2014). Coupled wind-forced controls of the Bering–Chukchi shelf circulation and the Bering Strait throughflow: Ekman transport, continental shelf waves, and variations of the Pacific–Arctic sea surface height gradient. *Progress in Oceanography*, *125*, 40–61. https://doi.org/10.1016/j.pocean.2014.04.006

Darby, D. A., & Bischof, J. F. (2004). A Holocene record of changing Arctic Ocean ice drift analogous to the effects of the Arctic Oscillation. *Paleoceanography*, *19*, PA1027. https://doi.org/10.1029/2003PA000961

Darby, D. A., Myers, W. B., Jakobsson, M., & Rigor, I. (2011). Modern dirty sea ice characteristics and sources: The role of anchor ice. *Journal of Geophysical Research*, *19*, PA1027. https://doi.org/10.1029/2003PA000961

Darby, D. A., Ortiz, J., Polyak, L., Lund, S., Jakobsson, M., & Woodgate, R. A. (2009). The role of currents and sea ice in both slowly deposited central Arctic and rapidly deposited Chukchi-Alaskan margin sediments. *Global and Planetary Change*, *68*(1-2), 58–72. https://doi.org/10.1016/j.gloplacha.2009.02.007

Deschamps, C. E. (2018). Dynamique sédimentaire et paléocéanographique le long des margescontinentales des mers de Beaufort et des Tchouktches (océan Arctique) depuis la dernière déglaciation. (Doctoral dissertation). UQAR-ISMER, Rimouski.

Deschamps, C.-E., Montero-serrano, J.-C., & St-Onge, G. (2018). Sediment provenance changes in the western Arctic Ocean in response to ice-rafting, sea-level and oceanic circulation variations since the last deglaciation. *Geochemistry Geophysics Geosystems*, *19*, 2147–2165. https://doi.org/10.1029/2017GC007411

Deschamps, C.-E., St-Onge, G., Montero-Serrano, J.-C., & Polyak, L. (2018). Chronostratigraphy and spatial distribution of the Chukchi and Beaufort Sea's magnetic sediments since the last deglaciation. *Boreas*, *47*(2), 544–564. https://doi.org/10.1111/bor.12296

Dickson, R., Rudels, B., Dye, S., Karcher, M., Meincke, J., & Yashayaev, I. (2007). Current estimates of freshwater flux through Arctic and subarctic seas. *Progress in Oceanography*, *73*(3-4), 210–230. https://doi.org/10.1016/j.pocean.2006.12.003

Du, J., Haley, B. A., & Mix, A. C. (2016). Neodymium isotopes in authigenic phases, bottom waters and detrital sediments in the Gulf of Alaska and their implications for paleo-circulation reconstruction. *Geochimica et Cosmochimica Acta*, *193*, 14–35. https://doi.org/10.1016/j.gca.2016.08.005

Dyke, A. S. (2004). An outline of the deglaciation of North America with emphasis on central and northern Canada. *Quaternary Glaciations-Extent and Chronology, Part II: North America*, *2b*, 373–424. https://doi.org/10.1016/S1571-0866(04)80209-4

Eberl, D. D. (2003). User guide to RockJock—A program for determining quantitative mineralogy from X-ray diffraction data. USGS Open File Report, OF 03-78, 40.

Forest, A., Osborne, P. D., Fortier, L., Sampei, M., & Lowings, M. G. (2015). Physical forcings and intense shelf-slope fluxes of particulate matter in the halocline waters of the Canadian Beaufort Sea during winter. *Continental Shelf Research*, *101*, 1–21. https://doi.org/10.1016/j.csr.2015.03.009

Forest, A., Tremblay, J. É., Gratton, Y., Martin, J., Gagnon, J., Darnis, G., et al. (2011). Biogenic carbon flows through the planktonic food web of the Amundsen Gulf (Arctic Ocean): A synthesis of field measurements and inverse modeling analyses. *Progress in Oceanography*, *91*(4), 410–436. https://doi.org/10.1016/j.pocean.2011.05.002

Frank, M. (2002). Radiogenic isotopes: Tracers of past ocean circulation and erosional input. *Reviews of Geophysics*, *40*(1), 1001. https://doi.org/10.1029/2000RG000094

Gamboa, A., Montero-Serrano, J.-C., St-Onge, G., Rochon, A., & Desiage, P.-A. (2017). Mineralogical, geochemical and magnetic signatures of surface sediments from the Canadian Beaufort Shelf and Amundsen Gulf (Canadian Arctic). *Geochemistry, Geophysics, Geosystems*, *18*, 488–512. https://doi.org/10.1002/2016GC006477

Grebmeier, J. M., Cooper, L. W., Feder, H. M., & Sirenko, B. I. (2006). Ecosystem dynamics of the Pacific-influenced northern Bering and Chukchi Seas in the Amerasian Arctic. *Progress in Oceanography*, *71*(2-4), 331–361. https://doi.org/10.1016/j.pocean.2006.10.001

Gutjahr, M., Frank, M., Lippold, J., & Halliday, A. N. (2014). Peak Last Glacial weathering intensity on the North American continent recorded by the authigenic Hf isotope composition of North Atlantic deep-sea sediments. *Quaternary Science Reviews*, *99*, 97–111. https://doi.org/10.1016/j.quascirev.2014.06.022

Gutjahr, M., Frank, M., Stirling, C. H., Klemm, V., van de Flierdt, T., & Halliday, A. N. (2007). Reliable extraction of a deepwater trace metal isotope signal from Fe-Mn oxyhydroxide coatings of marine sediments. *Chemical Geology*, *242*(3-4), 351–370. https://doi.org/10.1016/j.chemgeo.2007.03.021

Gutjahr, M., Hoogakker, B. a. a., Frank, M., & McCave, I. N. (2010). Changes in North Atlantic Deep Water strength and bottom water masses during Marine Isotope Stage 3 (45-35kaBP). *Quaternary Science Reviews*, *29*(19-20), 2451–2461. https://doi.org/10.1016/j.quascirev.2010.02.024

Haley, B. A., Du, J., Abbott, A. N., & McManus, J. (2017). The impact of benthic processes on rare earth element and neodymium isotope distributions in the oceans. *Frontiers in Marine Science*, *4*. https://doi.org/10.3389/fmars.2017.00426

Haley, B. A., Frank, M., Spielhagen, R. F., & Fietzke, J. (2008). Radiogenic isotope record of Arctic Ocean circulation and weathering inputs of the past 15 million years. *Paleoceanography*, *23*, PA1S13. https://doi.org/10.1029/2007PA001486

Haley, B. A., Klinkhammer, G. P., & McManus, J. (2004). Rare earth elements in pore waters of marine sediments. *Geochimica et Cosmochimica Acta*, *68*(6), 1265–1279. https://doi.org/10.1016/j.gca.2003.09.012

Haley, B. A., & Polyak, L. (2013). Pre-modern Arctic Ocean circulation from surface sediment neodymium isotopes. *Geophysical Research Letters*, *40*, 893–897. https://doi.org/10.1002/grl.50188

Harada, N., Katsuki, K., Nakagawa, M., Matsumoto, A., Seki, O., Addison, J. A., et al. (2014). Holocene sea surface temperature and sea ice extent in the Okhotsk and Bering Seas. *Biogeochemical and physical processes in the Sea of Okhotsk and the linkages to the Pacific Ocean*, *126*, 242–253. https://doi.org/10.1016/j.pocean.2014.04.017

Hill, J. C., & Driscoll, N. W. (2008). Paleodrainage on the Chukchi shelf reveals sea level history and meltwater discharge. *Marine Geology*, *254*(3-4), 129–151. https://doi.org/10.1016/j.margeo.2008.05.018

Hirano, D., Fukamachi, Y., Ohshima, K. I., Watanabe, E., Mahoney, A. R., Eicken, H., et al. (2018). Winter water formation in coastal polynyas of the eastern Chukchi shelf: Pacific and Atlantic influences. *Journal of Geophysical Research: Oceans*, *123*, 5688–5705. https://doi.org/10.1029/2017JC013307

Horikawa, K., Asahara, Y., Yamamoto, K., & Okazaki, Y. (2010). Intermediate water formation in the Bering Sea during glacial periods: Evidence from neodymium isotope ratios. *Geology*, *38*(5), 435–438. https://doi.org/10.1130/G30225.1

Horikawa, K., Martin, E. E., Basak, C., Onodera, J., Seki, O., Sakamoto, T., et al. (2015). Pliocene cooling enhanced by flow of low-salinity Bering Sea water to the Arctic Ocean. *Nature Communications*, *6*(1), 7587. https://doi.org/10.1038/ncomms8587

Jacobsen, S. B., & Wasserburg, G. J. (1980). Sm-Nd isotopic evolution of chondrites. *Earth and Planetary Science Letters*, *50*(1), 139–155. https://doi.org/10.1016/0012-821X(80)90125-9

Jakobsson, M., Pearce, C., Cronin, T. M., Backman, J., Anderson, L. G., Barrientos, N., et al. (2017). Post-glacial flooding of the Beringia Land Bridge dated to 11 cal ka BP based on new geophysical and sediment records. *Climate of the Past Discussions*, *13*(8), 991–1005. https://doi.org/10.5194/cp-13-991-2017

Jang, K., Huh, Y., & Han, Y. (2017). Authigenic Nd isotope record of North Pacific Intermediate Water formation and boundary exchange on the Bering Slope. *Quaternary Science Reviews*, *156*, 150–163. https://doi.org/10.1016/j.quascirev.2016.11.032

Jeandel, C., Arsouze, T., Lacan, F., Téchiné, P., & Dutay, J. C. (2007). Isotopic Nd compositions and concentrations of the lithogenic inputs into the ocean: A compilation, with an emphasis on the margins. *Chemical Geology*, *239*(1-2), 156–164. https://doi.org/10.1016/j.chemgeo.2006.11.013

Katsuki, K., Khim, B. K., Itaki, T., Harada, N., Sakai, H., Ikeda, T., et al. (2009). Land-sea linkage of Holocene paleoclimate on the southern Bering continental shelf. *Holocene*, *19*(5), 747–756. https://doi.org/10.1177/0959683609105298

Kinnard, C., Zdanowicz, C. M., Fisher, D. A., Isaksson, E., de Vernal, A., & Thompson, L. G. (2011). Reconstructed changes in Arctic sea ice over the past 1,450 years. *Nature*, *479*(7374), 509–512. https://doi.org/10.1038/nature10581

Kobayashi, D., Yamamoto, M., Irino, T., Nam, S.-I., Park, Y.-H., Harada, N., et al. (2016). Distribution of detrital minerals and sediment color in western Arctic Ocean and northern Bering Sea sediments: Changes in the provenance of western Arctic Ocean sediments since the last glacial period. *Polar Science*, *10*(4), 519–531. https://doi.org/10.1016/j.polar.2016.07.005

Lacan, F., & Jeandel, C. (2005). Neodymium isotopes as a new tool for quantifying exchange fluxes at the continent-ocean interface. *Earth and Planetary Science Letters*, *232*(3-4), 245–257. https://doi.org/10.1016/j.epsl.2005.01.004

Lambeck, K., Rouby, H., Purcell, A., Sun, Y., & Sambridge, M. (2014). Sea level and global ice volumes from the Last Glacial Maximum to the Holocene. *Proceedings of the National Academy of Sciences*, *111*(43), 15296–15303. https://doi.org/10.1073/pnas.1411762111

Li, C.-F., Guo, J.-H., Yang, Y.-H., Chu, Z.-Y., & Wang, X.-C. (2014). Single-step separation scheme and high-precision isotopic ratios analysis of Sr–Nd–Hf in silicate materials. *Journal of Analytical Atomic Spectrometry*, *29*(8), 1467–1476. https://doi.org/10.1039/C3JA50384D

Liu, Z., Yoshimura, K., Bowen, G. J., Buenning, N. H., Risi, C., Welker, J. M., & Yuan, F. (2014). Paired oxygen isotope records reveal modern North American atmospheric dynamics during the Holocene. *Nature Communications*, *5*(1), 1–7. https://doi.org/10.1038/ncomms4701

Maccali, J., Hillaire-Marcel, C., Carignan, J., & Reisberg, L. C. (2013). Geochemical signatures of sediments documenting Arctic sea-ice and water mass export through Fram Strait since the Last Glacial Maximum. *Quaternary Science Reviews*, *64*, 136–151. https://doi.org/10.1016/j.quascirev.2012.10.029

Maccali, J., Hillaire-Marcel, C., & Not, C. (2018). Radiogenic isotope (Nd, Pb, Sr) signatures of surface and sea ice-transported sediments from the Arctic Ocean under the present interglacial conditions. *Polar Research*, *37*(1), 1442982. https://doi.org/10.1080/17518369.2018.1442982

McKay, J. L., de Vernal, A., Hillaire-Marcel, C., Not, C., Polyak, L., & Darby, D. (2008). Holocene fluctuations in Arctic sea-ice cover: Dinocyst-based reconstructions for the eastern Chukchi Sea. *Canadian Journal of Earth Sciences*, *45*(11), 1377–1397. https://doi.org/10.1139/E08-046

Meinhardt, A.-K., März, C., Schuth, S., Lettmann, K. A., Schnetger, B., Wolff, J.-O., & Brumsack, H.-J. (2016). Diagenetic regimes in Arctic Ocean sediments: Implications for sediment geochemistry and core correlation. *Geochimica et Cosmochimica Acta*, *188*, 125–146. https://doi.org/10.1016/j.gca.2016.05.032

Molina-Kescher, M., Frank, M., & Hathorne, E. C. (2014). Nd and Sr isotope compositions of different phases of surface sediments in the South Pacific: Extraction of seawater signatures, boundary exchange, and detrital/dust provenance. *Geochemistry, Geophysics, Geosystems*, *15*, 3502–3520. https://doi.org/10.1002/2014GC005443

Montero-Serrano, J.-C., Bout-Roumazeilles, V., Tribovillard, N., Sionneau, T., Riboulleau, A., Bory, A., & Flower, B. (2009). Sedimentary evidence of deglacial megafloods in the northern Gulf of Mexico (Pigmy Basin). *Quaternary Science Reviews*, *28*(27), 3333–3347.

Nelson, H., & Creager, J. S. (1977). Displacement of Yukon-derived sediment from the Bering Sea to the Chukchi Sea during Holocene time. *Geology*, *5*(3), 141–146. https://doi.org/10.1130/0091-7613(1977)5<141:DOYSFB>2.0.CO;2

Nowell, G. M., Kempton, P. D., Noble, S. R., Saunders, a. D., Mahoney, J. J., & Taylor, R. N. (1998). High-precision Hf isotopic measurements of MORB and OIB by thermal ionization mass-spectrometry: Insights into the depleted mantle. *Chemical Geology*, *149*(3-4), 211–233. https://doi.org/10.1016/S0009-2541(98)00036-9

Okkonen, S. R., Ashjian, C. J., Campbell, R. G., Maslowski, W., Clement-Kinney, J. L., & Potter, R. (2009). Intrusion of warm Bering/Chukchi waters onto the shelf in the western Beaufort Sea. *Journal of Geophysical Research*, *114*, C00A11. https://doi.org/10.1029/2008JC004870

Osborne, P. D., & Forest, A. (2016). Sediment dynamics from coast to slope—Southern Canadian Beaufort Sea. In: Vila-Concejo, A.; Bruce, E.; Kennedy, D.M., and McCarroll, R.J. (eds.), Proceedings of the 14th International Coastal Symposium (Sydney, Australia). *Journal of Coastal Research*, *75*, 537–541.

Pearce, C. R., Jones, M. T., Oelkers, E. H., Pradoux, C., & Jeandel, C. (2013). The effect of particulate dissolution on the neodymium (Nd) isotope and Rare Earth Element (REE) composition of seawater. *Earth and Planetary Science Letters*, *369-370*, 138–147. https://doi.org/10.1016/j.epsl.2013.03.023

Petschick, R. (2000). MacDiff 4.2. 5 Manual. Institut für Geologie, Universität Erlangen: Germany.

Pickart, R. S. (2004). Shelfbreak circulation in the Alaskan Beaufort Sea: Mean structure and variability. *Journal of Geophysical Research*, *109*, C04024. https://doi.org/10.1029/2003JC001912

Pickart, R. S., Weingartner, T. J., Pratt, L. J., Zimmermann, S., & Torres, D. J. (2005). Flow of winter-transformed Pacific water into the Western Arctic. *Deep-Sea Research Part II: Topical Studies in Oceanography*, *52*(24-26), 3175–3198. https://doi.org/10.1016/j.dsr2.2005.10.009

Poirier, R. K., Cronin, T. M., Briggs, W. M., & Lockwood, R. (2012). Central Arctic paleoceanography for the last 50kyr based on ostracode faunal assemblages. *Marine Micropaleontology*, *88-89*, 65–76. https://doi.org/10.1016/j.marmicro.2012.03.004

Polyak, L., Belt, S. T., Cabedo-Sanz, P., Yamamoto, M., & Park, Y.-H. (2016). Holocene sea-ice conditions and circulation at the Chukchi-Alaskan margin, Arctic Ocean, inferred from biomarker proxies. *The Holocene*, *26*(11), 1810–1821. https://doi.org/10.1177/0959683616645939

Polyakov, I. V., Pnyushkov, A. V., Alkire, M. B., Ashik, I. M., Baumann, T. M., Carmack, E. C., et al. (2017). Greater role for Atlantic inflows on sea-ice loss in the Eurasian Basin of the Arctic Ocean. *Science*, *356*(6335), 285–291. https://doi.org/10.1126/science.aai8204

Porcelli, D., Andersson, P. S., Baskaran, M., Frank, M., Björk, G., & Semiletov, I. (2009). The distribution of neodymium isotopes in Arctic Ocean basins. *Geochimica et Cosmochimica Acta*, *73*(9), 2645–2659. https://doi.org/10.1016/j.gca.2008.11.046

Rickli, J., Frank, M., Baker, A. R., Aciego, S., de Souza, G., Georg, R. B., & Halliday, A. N. (2010). Hafnium and neodymium isotopes in surface waters of the eastern Atlantic Ocean: Implications for sources and inputs of trace metals to the ocean. *Geochimica et Cosmochimica Acta*, *74*(2), 540–557. https://doi.org/10.1016/j.gca.2009.10.006

Rickli, J., Frank, M., & Halliday, A. N. (2009). The hafnium–neodymium isotopic composition of Atlantic seawater. *Earth and Planetary Science Letters*, *280*(1-4), 118–127. https://doi.org/10.1016/j.epsl.2009.01.026

Rudels, B., Jones, E. P., Schauer, U., & Eriksson, P. (2004). Atlantic sources of the Arctic Ocean Halocline. *Polar Research*, *23*(2), 181–208. https://doi.org/10.1111/j.1751-8369.2004.tb00007.x

Schoster, F., Behrends, M., Muller, R., Stein, R., & Washner, M. (2000). Modern river discharge and pathways of supplied material in the Eurasian Arctic Ocean: Evidence from mineral assemblages and major and minor element distribution. *International Journal of Earth Sciences*, *89*(3), 486–495. https://doi.org/10.1007/s005310000120

Screen, J. A., & Francis, J. A. (2016). Contribution of sea-ice loss to Arctic amplification is regulated by Pacific Ocean decadal variability. *Nature Climate Change*, *6*(9), 856–860. https://doi.org/10.1038/nclimate3011

Serreze, M. C., Holland, M. M., & Stroeve, J. (2007). Perspectives on the Arctic's shrinking sea-ice cover. *Science*, *315*(5818), 1533–1536. https://doi.org/10.1126/science.1139426

Shimada, K., Kamoshida, T., Itoh, M., Nishino, S., Carmack, E., McLaughlin, F., et al. (2006). Pacific Ocean inflow: Influence on catastrophic reduction of sea ice cover in the Arctic Ocean. *Geophysical Research Letters*, *33*, L08605. https://doi.org/10.1029/2005GL025624

Stein, R., Fahl, K., Schade, I., Manerung, A., Wassmuth, S., Niessen, F., & Nam, S.-I. (2017). Holocene variability in sea ice cover, primary production, and Pacific-Water inflow and climate change in the Chukchi and East Siberian Seas (Arctic Ocean). *Journal of Quaternary Science*, *32*(3), 362–379. https://doi.org/10.1002/jqs.2929

Stichel, T., Frank, M., Rickli, J., & Haley, B. A. (2012). The hafnium and neodymium isotope composition of seawater in the Atlantic sector of the Southern Ocean. *Earth and Planetary Science Letters*, *317-318*, 282–294. https://doi.org/10.1016/j.epsl.2011.11.025

Tachikawa, K., Jeandel, C., Vangriesheim, A., & Dupré, B. (1999). Distribution of rare earth elements and neodymium isotopes in suspended particles of the tropical Atlantic Ocean (EUMELI site). *Deep-Sea Research Part I: Oceanographic Research Papers*, *46*(5), 733–755. https://doi.org/10.1016/S0967-0637(98)00089-2

Tanaka, T., Togashi, S., Kamioka, H., Amakawa, H., Kagami, H., Hamamoto, T., et al. (2000). JNdi-1: A neodymium isotopic reference in consistency with LaJolla neodymium. *Chemical Geology*, *168*(3-4) 279–281.

Taylor, S. R., & McClennan, S. M. (1985). *The continental crust: Its composition and evolution* (pp. 312–312). Oxford: John Wiley & Sons Ltd.
VanLaningham, S., Pisias, N. G., Duncan, R. A., & Clift, P. D. (2009). Glacial–interglacial sediment transport to the Meiji Drift, northwest Pacific Ocean: Evidence for timing of Beringian outwashing. *Earth and Planetary Science Letters*, *277*(1–2), 64–72. https://doi.org/10.1016/j.epsl.2008.09.033
Vervoort, J. D., Patchett, P. J., Blichert-toft, J., & Albare, F. (1999). Relationships between Lu-Hf and Sm-Nd isotopic systems in the global sedimentary system. *Earth and Planetary Science Letters*, *168*(1-2), 79–99. https://doi.org/10.1016/S0012-821X(99)00047-3
Wagner, A., Lohmann, G., & Prange, M. (2011). Arctic river discharge trends since 7 ka BP. *Global and Planetary Change*, *79*(1-2), 48–60. https://doi.org/10.1016/j.gloplacha.2011.07.006
Wahsner, M., Müller, C., Stein, R., Ivanov, G., Levitan, M., Shelekhova, E., & Tarasov, G. (1999). Clay-mineral distribution in surface sediments of the Eurasian Arctic Ocean and continental margin as indicator for source areas and transport pathways—A synthesis. *Boreas*, *28*(1), 215–233. https://doi.org/10.1111/j.1502-3885.1999.tb00216.x
Wanner, H., Beer, J., Bütikofer, J., Crowley, T. J., Cubasch, U., Flückiger, J., et al. (2008). Mid- to Late Holocene climate change: An overview. *Quaternary Science Reviews*, *27*(19-20), 1791–1828. https://doi.org/10.1016/j.quascirev.2008.06.013
Weingartner, T., Aagaard, K., Woodgate, R., Danielson, S., Sasaki, Y., & Cavalieri, D. (2005). Circulation on the north central Chukchi Sea shelf. *Deep Sea Research Part II: Topical Studies in Oceanography*, *52*(24-26), 3150–3174. https://doi.org/10.1016/j.dsr2.2005.10.015
Weis, D., Kieffer, B., Maerschalk, C., Barling, J., De Jong, J., Williams, G. A., et al. (2006). High-precision isotopic characterization of USGS reference materials by thermal ionization mass spectrometer and MC-ICP-MS. *Geochemistry, Geophysics, Geosystems*, *7*, Q08006. https://doi.org/10.1029/2006GC001283
Wickert, A. D. (2016). Reconstruction of North American drainage basins and river discharge since the Last Glacial Maximum. *Earth Surface Dynamics*, *4*, 1–50. https://doi.org/10.5194/esurf-2016-8
Wilson, D. J., Piotrowski, A. M., Galy, A., & Clegg, J. A. (2013). Reactivity of neodymium carriers in deep sea sediments: Implications for boundary exchange and paleoceanography. *Geochimica et Cosmochimica Acta*, *109*, 197–221. https://doi.org/10.1016/j.gca.2013.01.042
Winsor, P., & Chapman, D. C. (2004). Pathways of Pacific water across the Chukchi Sea: A numerical model study. *Journal of Geophysical Research*, *109*, C03002. https://doi.org/10.1029/2003JC001962
Woodgate, R. A., Aagaard, K., Swift, J. H., Falkner, K. K., & Smethie, W. M. (2005). Pacific ventilation of the Arctic Ocean's lower halocline by upwelling and diapycnal mixing over the continental margin. *Geophysical Research Letters*, *32*, L18609. https://doi.org/10.1029/2005GL023999
Yamamoto, M., Nam, S.-I., Polyak, L., Kobayashi, D., Suzuki, K., Irino, T., & Shimada, K. (2017). Holocene dynamics in the Bering Strait inflow to the Arctic and the Beaufort Gyre circulation based on sedimentary records from the Chukchi Sea. *Climate of the Past*, *13*(9), 1111–1127. https://doi.org/10.5194/cp-13-1111-2017
Zhang, L., & Delworth, T. L. (2015). Analysis of the characteristics and mechanisms of the Pacific decadal oscillation in a suite of coupled models from the geophysical fluid dynamics laboratory. *Journal of Climate*, *28*(19), 7678–7701. https://doi.org/10.1175/JCLI-D-14-00647.1
Zimmermann, B., Porcelli, D., Frank, M., Andersson, P. S., Baskaran, M., Lee, D.-C., & Halliday, A. N. (2009). Hafnium isotopes in Arctic Ocean water. *Geochimica et Cosmochimica Acta*, *73*(11), 3218–3233. https://doi.org/10.1016/j.gca.2009.02.028
Zimmermann, B., Porcelli, D., Frank, M., Rickli, J., Lee, D.-C., & Halliday, A. N. (2009). The hafnium isotope composition of Pacific Ocean water. *Geochimica et Cosmochimica Acta*, *73*(1), 91–101. https://doi.org/10.1016/j.gca.2008.09.033

References From the Supporting Information

Andrews, J. T., Stein, R., Moros, M., & Perner, K. (2016). Late Quaternary changes in sediment composition on the NE Greenland margin (~73° N) with a focus on the fjords and shelf. *Boreas*, *45*(3), 381–397. https://doi.org/10.1111/bor.12169
Funk, J. A. (2004). Sediment accumulation and diagenesis in the Late Quaternary equatorial Atlantic Ocean: An environmental magnetic and geochemical perspective. Ph.D. thesis, Universitat Bremen. 103 p.
Hofmann, D. I., & Fabian, K. (2009). Correcting relative paleointensity records for variations in sediment composition: Results from a South Atlantic stratigraphic network. *Earth and Planetary Science Letters*, *284*(1-2), 34–43. https://doi.org/10.1016/j.epsl.2009.03.043
Hofmann, D. I., Fabian, K., Schmieder, F., Donner, B., & Bleil, U. (2005). A stratigraphic network across the Subtropical Front in the central South Atlantic: Multi-parameter correlation of magnetic susceptibility, density, X-ray fluorescence and ^{18}O records. *Earth and Planetary Science Letters*, *240*(3-4), 694–709. https://doi.org/10.1016/j.epsl.2005.09.048
Macdonald, R. W., & Gobeil, C. (2012). Manganese sources and sinks in the Arctic Ocean with reference to periodic enrichments in basin sediments. *Aquat. Geochem.*, *18*(6), 565–591. https://doi.org/10.1007/s10498-011-9149-9
Meinhardt, A. K., Pahnke, K., Böning, P., Schnetger, B., & Brumsack, H. J. (2016). Climate change and response in bottom water circulation and sediment provenance in the Central Arctic Ocean since the Last Glacial. *Chemical Geology*, *427*, 98–108. https://doi.org/10.1016/j.chemgeo.2016.02.019